Abstract of thesis entitled

'Post-buckling Analysis of Plates and Struts

with Initial Imperfection'

submitted by

LUI TAI HONG

for the degree of

Master of Philosophy

at the Hong Kong Polytechnic University

in May 2000

ABSTRACT

Computational procedures for predicting the post-buckling responses of struts and plates with general initial imperfections, when subjected to progressive end shortening, are developed. Geometric non-linearity is introduced into the strain-displacement relations in a manner consistent with the von Karman assumptions. The set of non-linear equilibrium equations is solved by a Newton-Raphson procedure.

In the post-buckling analysis of struts, the actual initial imperfection is simulated by suitable polynomial function, while the deformations are expressed by Fourier series. Transverse shear effect is included in the formulation. Comparisons with classical solutions without transverse shear and experimental results are presented.

In the context of classical plate theory, a finite strip approach is developed for predicting the post-buckling response of plates under uniform end shortening. Out-of-plane initial imperfection is represented by a set of polynomial functions in the longitudinal direction, which are interpolated by some crosswise functions in the transverse direction. The approach is very general and is applicable to anisotopic plates and plates with general shapes of initial imperfection.

Applications on perfectly flat plates and plates with various forms of initial imperfections are considered. It is demonstrated that both the post-buckling behaviors and deformed shapes are strongly influenced by the magnitudes and shapes of the initial imperfections.

DECLARATION

I hereby declare that this thesis entitled 'Post-buckling Analysis of Plates and Struts with Initial Imperfection' has not been previously submitted to any other institution for a degree or other qualification, and contains no material previously published or written by another person, except where due reference is made in the text.

_____

Lui, Tai-hong

ACKNOWLEDGEMENTS

During the past two years, under the supervision of my supervisor, Dr. Lam, S. S. E., I have been consistently enriched with his delightful inspiration and warm-hearted encouragement, and I would very much like to take this opportunity to express my truest gratitude to him. It would have been very difficult, if not impossible, to finish this study should I have failed to receive his enthusiasm and kind guidance. I would also like to thank my co-supervisor, Prof. Ko, J. M., for his kind support.

A special note of thanks goes to Dr. Zou, G. P., who devoted his time and sincere concern to advice me on programming. His assistance has definitely contributed a lot to this project.

My gratefulness would not fail to go to Dr. Chung, K. F., for all his demonstrations of practical applications, which help me turn abstract ideas and estimations into invaluable visual experiences, as well as reminding me the aphorism: 'seeing is believing'.

Finally, I would also like to thank my family for every dedication I can never forget nor aptly express.

TABLE OF CONTENTS

TABLE OF CONTENTS (Continued)

LIST OF NOTATIONS

a_i, a_{ij}	Coefficients of polynomial for initial imperfection
A	Cross-sectional area of a strut, length of a plate
$\boldsymbol{A}$, $\boldsymbol{B}$, $\boldsymbol{D}$	Stiffness coefficients
$\boldsymbol{b}_e$, $\boldsymbol{B}_L$, $\boldsymbol{B}_{NL}$, $\boldsymbol{B}_I$, $\boldsymbol{B}_\chi$	Strain components in matrix forms
B, b	Widths of a plate and a finite strip
ds, dx, dz	Original lengths of a line element and its components in x and z directions
ds_a, dx_a, dz_a	Lengths of a line element and its components in x and z directions after deformation
$\boldsymbol{d}$, $\boldsymbol{d}$	Displacement coefficient vector and its correction vector
$\boldsymbol{d}_p$, $\boldsymbol{d}_b$	Coefficient vectors for in-plane and out-of-plane displacements
D, D_{slope}	Sum of square differences between the actual and approximate initial imperfections due to the magnitude and slope
$\boldsymbol{e}$	End-shortening strain
E	Modulus of elasticity
$f(x)$, $f_I(x)$	Approximate forms of initial imperfection
F	Non-dimensional load factor
F_x	Average force over the length of a strut
$F(x)$, $F_I(x)$	Actual forms of initial imperfection
$g_I(y)$	Crosswise polynomial function with displacement coefficients
G	Shear modulus
h	Thickness
I	Second moment of area
k	Shear correction factor

$\boldsymbol{K}$, $\boldsymbol{K}_T$	Tangent stiffness matrices
L	Length of a strut
$\boldsymbol{M}$	Bending and twisting stress
N_{av}	Average longitudinal force
$N_m(y)$, $\hat{N}_m(y)$	Shape functions
$\boldsymbol{N}$	Direct and shearing stress
$\boldsymbol{R}$	Unbalance force or error
u, v, w	Displacements in x, y and z directions on the middle surface
$\bar{u}$, $\bar{v}$, $\bar{w}$	Displacements in x, y and z directions at a general point
u_I, w_I, β_I	Coefficients for displacements u, w and β_x
u_{im}, v_{im}, w_{im}, ψ_{im}	Coefficients for displacements u, v, w and ψ along the nodal line m
$U_i(x)$, $V_i(x)$, $W_i(x)$	Longitudinal displacement functions
V_i, $A_{ij}^{(p)}$, B_{ijm}, C_{ijm}, D_{ijmn}	Coefficients of energy equation for a strut
w_i^*, b_i^*	Coefficients for displacements w and β_x in finite element representation
w_o	Initial imperfection
w_{oh}	Magnitude of initial imperfection
w_t	Total deflection
x'	Location of maximum initial imperfection
α	Parameter for lateral displacement at loaded ends
β_x	Rotation along the strut
δ_{ij}	Kronecker delta
ε_o	Prescribed end-shortening strain

ε_x, $\bar{\varepsilon}_x$	Axial strains in x direction on the middle surface and at a general point
ε, χ	In-plane and bending strains
ε_{ave}	Average strain
ε_I	Strain component due to the initial imperfection
ε_L, ε_{NL}	Linear and non-linear strain components
γ_x, γ_{yz}, γ_{zx}	Through-thickness transverse shear strains
ν	Poisson's ratio
Π, Π_p	Total potential energy and potential energy of a finite strip
σ_x, χ_x	Normal and bending strains in x direction
τ	Shear stress, tolerance for convergence criterion
ψ_x, ψ_y	Rotations about x and y axes

LIST OF TABLES

LIST OF FIGURES

CHAPTHER 1

INTRODUCTION

1.1 OBJECTIVES OF STUDY

The aims of this study are to develop computational procedures for the prediction of the post-buckling response of struts and laminated plates with general initial imperfections. The main objectives are as follows:

a, To develop computational procedures for the post-buckling analysis of struts and plates with general initial imperfections when subjected to progressive end-shortening;

b, to examine the adaptability of using Fourier series and polynomial functions to represent the deformations and initial imperfections, respectively;

c, to include the transverse shear effect in the analysis of struts under axial compression, and to examine the transverse shear effect by comparing the responses of struts of various thickness; and

d, to investigate the effects of initial imperfection on the post-buckling response of laminated plates under end-shortening strain.

1.2 SCOPE OF STUDY

The present study includes the development of the finite strip method for the post-buckling analysis of struts and plates with

general initial imperfections. The procedures are codified in standard FORTRAN 90 and compiled by Lahey FORTRAN 90 v3.5 on a PC operated under Windows 98 environment. A number of applications have been studied to demonstrate the response of struts and plates under various conditions.

Background discussion and review on related literatures are presented in Chapter 2, which comprises review on the theories and procedures on non-linear structural analysis, means to approximate the initial imperfection as well as numerical techniques for solving partial differential equations and non-linear programming.

Post-buckling analysis of struts with general initial imperfection is presented in Chapter 3. Starting from the non-linear strain-displacement relationships, a formulation with transverse shear effect is developed. By using the least-squares technique, initial imperfections are simulated by polynomial functions. Numerical examples with symmetric and non-symmetric imperfections are presented. Struts with various thickness are also considered to examine the effect of transverse shear.

Chapter 4 gives an account on the analysis of laminated plates when subjected to progressive end-shortening strain. The formulation is based on the finite strip method and in the context of classical plate theory. The method of simulating the initial imperfection by polynomials described in Chapter 3 is extended to the analysis of plates.

Brief descriptions of the computer architecture and programming technique implementation to codify the finite strip procedures are presented in Chapter 5. Various applications are presented in Chapter 6. Post-buckling responses of isotopic plates and anisotropic laminates with symmetric and non-symmetric initial imperfection are considered.

Conclusions of the study are presented in Chapter 7. Some

recommendations on the computational effort and efficiency of the finite strip method, along with recommendations on further work to study shear deformable plates are also outlined in the concluding chapter.

CHAPTER 2

REVIEWS ON RELATED LITERATURE

Today, more and more structural components are made of laminated plates. This demonstrates the potential of laminate to be utilized as the main components in mechanical, aerospace, marine and other branches of engineering. Laminated plate has the advantages of lightness and good strength to thickness ratio. With feasibility in layup arrangement, design engineers are able to optimize a laminate for various applications. Accurate and efficient predictions on the post-buckling response of laminated plates are required to quantify the ultimate capacity needed for design. For structure under in-plane compression, a significant amount of research, Leissa (1987) and Kapania and Raciti (1989), has been conducted on their buckling and post-buckling behavior. A review on this aspect is as follows.

2.1 POST-BUCKLING ANALYSIS OF STRUTS AND PLATES

When an in-plane compression is applied to a strut or plate, lateral deformation is anticipated due to buckling. Among other, Timoshenko and Gere (1961) and Allen and Bulson (1980) have provided detail discussion on various types of buckling of strut and plate.

Consistent with the von Karman assumptions, for instances see Novozhilov (1953), geometric non-linearity is introduced into the strain-displacement relationships through the out-of-plane w terms, whilst the second order effect with respect to the in-plane

displacements u, v are usually neglected. A number of applications on the non-linear analysis of plates were demonstrated in the book by Chia (1980). Because of the presence of anisotropic material coupling terms in the stress-strain relationships, Whitney (1987), out-of-plane deformations are initiated by in-plane loading. Eigenvalue-type buckling may not necessarily occur even for a perfectly flat laminated plate subjected to an in-plane compression.

In the analysis of thin structures, the transverse shear effect is negligible, Novozhilov (1953), as shown in equations (2.1.1) and (2.1.2).

$$\gamma_{yz} = \frac{\partial w}{\partial y} + \psi_y \rightarrow 0 \qquad (2.1.1)$$

$$\gamma_{zx} = \frac{\partial w}{\partial x} + \psi_x \rightarrow 0 \qquad (2.1.2)$$

where γ_{yz} and γ_{zx} are the transverse shear strains, w is the out-of-plane deformation and ψ_x, ψ_y denote the rotations about the y and negative x axes, respectively.

In the context of classical plate theory, Chia and Prabhakara (1973), (1974) & (1975) conducted post-buckling analysis on plates using Fourier series approximations. Stein (1983) & (1985) analyzed and indicated the differences between the post-buckling responses of isotropic and orthotropic plates of various boundary conditions. Shin, Griffin and Gurdal (1993) determined the changes in buckled shapes of laminated plates subjected to progressive in-plane compression. Graves-Smith and Sridharan (1978) & (1981), Hancock (1981), Gierlinski and Graves-Smith (1984), Dawe, Lam and Azizian (1992), Azhari and Bradford (1995) & (1997) and Dawe and Wang (1998) also developed the finite strip approaches for thin plates

and thin plate structures with the transverse shear effect neglected.

When the thickness of a plate increases, transverse shear deformation, Whitney and Pagano (1970) and Whitney (1973), must be included. Equations (2.1.1) and (2.1.2) are no longer zeros. Mawenya and Davies (1974) demonstrated the effect of transverse shear by analyzing the bending of plates with various thickness. Hughes, Taylor and Kanoknukulchai (1977) developed a finite element approach for the analysis of plates with transverse shear effect. The formulation is also applicable to thin plates. Stein (1989) considered the difference between the traditional post-buckling results for thin plates with transverse shear effect and classical solutions. The transverse shear effects under various edge conditions were also examined. Using shear deformation plate theory, Lam, Dawe and Azizan (1993) studied the post-buckling response of laminated plates. Discussion on the shear locking effect, due to the inclusion of transverse shear deformation, can be found in Chapter 2.3.

2.2 INITIAL IMPERFECTIONS

Responses of struts and plates under axial loads are strongly influenced by the shapes and magnitudes of initial imperfections. Symmetric initial imperfections in the form of Fourier series or trigonometric functions have been considered by many researchers. Timoshenoko and Gere (1961) expressed the initial imperfections as Fourier series in the analysis of plates subjected to transverse loading. Yamaki (1959) proposed analytical solution for post-buckling behavior of isotropic plates with initial imperfection. The shapes of the initial imperfection and out-of-plate deformation

were assumed to be the same, which were symmetric and in the form of Fourier series. Similar representation was also applied by Shen and Williams (1995) for the analysis of laminated plates. Numerical examples of unsymmetric angle-ply and symmetric cross-ply laminates were presented. Comparisons between perfect and imperfect plates were also reported to indicate the effects of initial imperfection. Dawe, Wang and Lam (1995) applied the finite strip method and expressed the initial imperfection along each nodal line by Fourier series. The nodal imperfections were then interpolated by some crosswise polynomial functions. The representation of initial imperfection is consistent with the finite strip model and can be programmed easily. Formulations, based on both classical and shear deformation plate theories, were presented.

To represent the initial imperfection in general form, piecewise polynomial functions, which are readily applied to the finite element method, have been used. Among others, this approach was implemented by Saigal, Kapania and Yang (1986) to analyze imperfect laminated shell. Kapania and Yang (1987) further extended the work to study the buckling, post-buckling and vibrations of imperfect plates. A number of comparisons were made with other available solutions. By applying the least-squares technique, Lam (1998) simulated the initial imperfection of a strut by polynomial function, whilst the displacements were represented by Fourier series. The analytical results compared well with the experimental measurements. Using similar technique to represent the out-of-plane imperfection along each nodal line, Lui and Lam (1999) developed a finite strip approach for the post-buckling analysis of rectangular plates. This approach was further applied by Lui and Lam (1999) to investigate the responses of plates with various initial imperfections.

In order to quantify the effect of initial imperfection, other

approaches were introduced by Fraser and Budiansky (1969) and Elishakoff, Cai and Starnes (1994) to examine the buckling behavior of a column with random initial imperfection. Based on sensitivity studies, Ikeda and Murota (1990) & (1990) determined the critical initial imperfection for truss structures.

2.3 NUMERICAL TECHNIQUES

The finite element method, for instances see Zienkiewicz and Taylor (1989), is perhaps the most common numerical procedure for general applications. It is able to model structure with any geometry, boundary conditions and material variations. A review article about the developments in geometrically non-linear finite element analysis was given by Gallagher (1973). Saigal, Kapani and Yang (1986) and Kapania and Yang (1987) presented the non-linear analyses of imperfect shells and plates, respectively. When the conventional finite elements including the transverse shear effect are applied to the analysis of thin structures, shear locking effect occurs. This leads to a reduction in accuracy, Moy and Lam (1990). It is due to the existence of excess constraints in the limiting case of zero transverse shear strain when the thickness becomes relatively small, see equations (2.1.1) and (2.1.2). Several numerical techniques were proposed to overcome this problem. Zienkiewicz, Taylor and Too (1971) proposed the reduced integration technique. Hughes, Taylor and Kanoknukulchai (1977) presented the analysis of plate bending including the transverse shear effect. Two-point quadrature was employed in the bending term, whilst both one and two-point quadratures were considered in the shearing term. It was noted that accurate solutions were obtained on the applications of thin plate when one-point

quadrature was used to integrate the shearing term. Prathap and Bhashyam (1985) discussed the error due to the shear locking effect and compared with solutions using selective reduced integration.

The finite strip method, introduced by Cheung (1968), is well established for the analysis of single plates and prismatic plate structures. The two-dimensional displacement field is reduced to one-dimension with shape functions, as shown in equation (2.1.3).

$$w(x, y) = \sum_{i=1}^{m} W_i(x)\, N_i(y) \qquad (2.1.3)$$

where $W_i(x)$ is the displacement function along each longitudinal nodal line, $N_i(y)$ is the shape function in the transverse direction and m is the number of nodes in a finite strip. Some latest developments have been recorded in a recent reference by Cheung and Tham (1997). Comparisons in storage, accuracy and efficiency were made with the finite element method. It is noted that smaller number of equations and matrix with narrow bandwidth are usually anticipated when using the finite strip method. Mawenya and Davies (1974) applied the finite strip method for plate bending with transverse shear effect. Numerical examples of thin, thick and sandwich plates were presented. In order to diminish the shear locking effect, Hinton and Zienkiewicz (1977) and Onate and Suarez (1983) applied the reduced and selective integration techniques, respectively. Accuracy of linear and quadratic strips was improved and comparisons of the analyses of plates with various thickness were shown.

In the analysis of thin plates or thin plate structures, Graves-Smith and Sridharan (1978) & (1981) developed the finite strip approach in the context of classical plate theory. Applications on box columns of various sections were presented.

Comparisons with the finite element method on storage and efficiency were shown in tabulate form. Later, Gierlinski and Graves-Smith (1984) studied the behavior of thin-walled structures under various kinds of loading. Hancock (1981) proposed a non-linear analysis for imperfect thin plate structures. Examples of square plates and various types of thin-walled column were presented. Further works on the finite strip method including bubble function were recently developed by Azhari and Bradford (1995) & (1997).

Dawe, Lam and Azizian (1992) developed the finite strip for post-buckling analysis of laminated plates under end-shortening in the context of classical plate theory, of which displacements along each nodal line were expressed in the form of Fourier series. Isotropic plates, unsymmetric cross-ply and angle-ply laminates with various boundary conditions were considered. Further development on the analysis using shear deformation plate theory was proposed by Lam, Dawe and Azizian (1993). Results from the approaches by both theories and finite element solutions were compared. Summary of the work based on both theories can also be found in a contributed chapter, Lam and Dawe (1998). Post-local-buckling analysis of composite prismatic plate structures was then developed based on the above approaches, Dawe, Lam and Azizian (1993). Other modification for the analysis of imperfect laminated plates under end-shortening and normal pressure was presented by Dawe, Wang and Lam (1995). Lam, Zou and Lui (1999) developed a the load increment procedure for the post-buckling analysis of laminated plates. Dawe and Wang (1998) studied the post-buckling analysis of thin plate by the spline finite strip method, of which displacements along each nodal line were represented by cubic spline functions. It is beyond doubt that the finite strip method is now well matured as an analytical tool in the analysis of

prismatic structures.

In solving the non-linear problem, a number of numerical techniques have been developed. Descriptions on the solution methods generally used in non-linear analysis, including direct iterative method and Newton-Raphson method, were described by Cook, Malkus and Plesha (1989). Gisvold and Moe (1970) presented several traditional non-linear solution techniques applicable to buckling problem. Minguet, Dugundji and Lagace (1989) described various numerical minimization techniques, the steepest descent, conjugated gradient and Newton-Raphson methods, for the post-buckling analysis of laminated plates. Newton-Raphson method was also applied by Shiau and Wu (1995) and Dawe, Lam and Azizian (1998) for the post-buckling analysis of laminated plates and plate structures, respectively. The stable and unstable equilibrium paths were traced when a progressive compression load was applied. The changes in buckled shapes were also indicated. The above mentioned Newton-Raphson procedure has been proved to be highly reliable in predicting the geometrically non-linear response and will be adopted in this study as the core solution procedure.

CHAPTER 3

POST-BUCKLING ANALYSIS OF STRUTS WITH GENERAL INITIAL IMPERFECTION - TRANSVERSE SHEAR EFFECT

This chapter introduces a numerical approach for the post-buckling analysis of a strut subjected to progressive end-shortening strain, see Figure 3.1. The length and cross-section area of the strut are L and A, respectively. Both ends are simply supported and general initial imperfection $w_o(x)$ is allowed in the analysis.

$u(x)$ and $w(x)$ denote the axial and lateral displacements, respectively. Under the consideration of transverse shear effect, rotation $\beta_x(x)$ is also included. Polynomial functions and Fourier series are used to represent the initial imperfection and displacements, respectively. In previous work, Lam (1998) has neglected the transverse shear effect which is now included in the study. Some comparisons between the results by the present and previous approaches are made to indicate the effect of transverse shear. Finally, discussion about the efficiency of the present approach is also included.

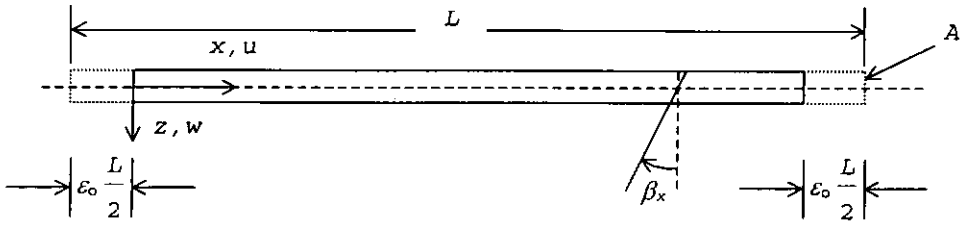

Figure 3.1 Strut under end-shortening strain ε_o

3.1 STRAIN-DISPLACEMENT RELATIONSHIPS AND ENERGY EQUATIONS

Consistent with the von Karman assumptions, for instances see Novozhilov (1953), the non-linear strain-displacement relationships of a strut can be derived by considering the deformation of a line element parallel to the x-axis, as shown in Figure 3.2. Here, ds is the original length of the line element, and dx, dz are the lengths in the x, z directions, respectively. ds_a, dx_a and dz_a are the lengths after deformation. Subscripts a denote the variables after deformation. (x, z) and $(\bar{u}, \bar{w})$ are the coordinates and displacements, in x and z directions, at a general point.

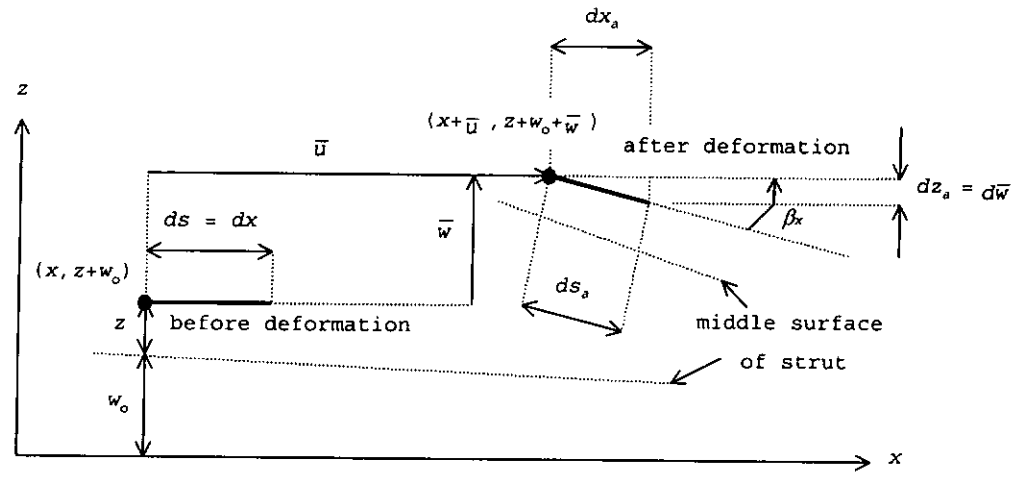

Figure 3.2 Deformation of a line element parallel to x-axis

From Figure 3.2, it can be deduced that

$$x_a = x + \bar{u}\ ; \qquad z_a = z + \bar{w} + w_o \tag{3.1.1}$$

$$\frac{dx_a}{dx} = 1 + \frac{d\bar{u}}{dx}\ ; \qquad \frac{dz_a}{dx} = \frac{d\bar{w}}{dx} + \frac{dw_o}{dx} \tag{3.1.2}$$

$$ds_a^2 = dx_a^2 + dz_a^2 \quad \text{(Pythagorean Theorem)} \tag{3.1.3}$$

$$\left(\frac{ds_a}{dx}\right)^2 - 1 = 2\frac{d\bar{u}}{dx} + \left(\frac{d\bar{u}}{dx}\right)^2 + \left(\frac{d\bar{w}}{dx}\right)^2 + 2\frac{d\bar{w}}{dx}\frac{dw_o}{dx} + \left(\frac{dw_o}{dx}\right)^2 \tag{3.1.4}$$

Let $\bar{\varepsilon}_x$ be the axial strain at a general point,

$$\bar{\varepsilon}_x = \frac{ds_a - ds}{ds} = \frac{ds_a - dx}{dx} \tag{3.1.5}$$

$$\bar{\varepsilon}_x + \frac{1}{2}(\bar{\varepsilon}_x)^2 = \frac{1}{2}\left[\left(\frac{ds_a}{dx}\right)^2 - 1\right] \tag{3.1.6}$$

Using equation (3.1.4) and neglecting the terms $(\bar{\varepsilon}_x)^2$, $(d\bar{u}/dx)^2$ and $(dw_o/dx)^2$, we have

$$\bar{\varepsilon}_x = \frac{d\bar{u}}{dx} + \frac{1}{2}\left(\frac{d\bar{w}}{dx}\right)^2 + \frac{d\bar{w}}{dx}\frac{dw_o}{dx} \tag{3.1.7}$$

For the variables at the middle surface (without the overhead bar),

$$\bar{u} = u + z\beta_x ; \qquad \bar{w} = w \tag{3.1.8}$$

$$\beta_x = \frac{-dz_a}{ds_a} = \frac{-dw}{dx + \delta} \tag{3.1.9}$$

$$\beta_x = -\frac{dw}{dx} + \gamma_x \tag{3.1.10}$$

where γ_x is the transverse shear strain which is introduced to account for the transverse shear effect. In equations (3.1.9) and (3.1.10), δ and γ_x vanish if the shear effect is neglected.

Substitute equation (3.1.8) into equation (3.1.7),

$$\bar{\varepsilon}_x = \frac{du}{dx} + z\frac{d\beta_x}{dx} + \frac{1}{2}\left(\frac{dw}{dx}\right)^2 + \frac{dw}{dx}\frac{dw_o}{dx} \tag{3.1.11}$$

Consistent with the relationships between the strain at a general point and at the middle surface,

$$\bar{\varepsilon}_x = \varepsilon_x + z\frac{d\beta_x}{dx} = \varepsilon_x + z\chi_x \tag{3.1.12}$$

The non-linear strain-displacement relationships become

$$\varepsilon_x = \frac{du}{dx} + \frac{1}{2}\left(\frac{dw}{dx}\right)^2 + \frac{dw_o}{dx}\frac{dw}{dx} \tag{3.1.13}$$

$$\chi_x = \frac{d\beta_x}{dx} \tag{3.1.14}$$

$$\gamma_x = \beta_x + \frac{dw}{dx} \tag{3.1.15}$$

The constitutive stress-strain relations are defined as

$$\sigma_x(x, z) = E(\varepsilon_x + z\chi_x) \tag{3.1.16}$$

$$\tau(x) = \frac{G}{k}\gamma_x \tag{3.1.17}$$

where $\sigma_x(x, z)$ is the stress in x direction, $\tau(x)$ is the shear stress, E and G are modulus of elasticity and shear modulus respectively. z is the through-thickness coordinate. In the above expressions, the transverse shear strain is assumed to be uniform through the thickness. Shear correction factor k is introduced to allow for the fact that actual through-thickness transverse shear strain distribution is not uniform. Appropriate values of shear correction factor can be determined using the method proposed by Whitney (1973) & (1987). For isotropic material, the shear correction factor k = 1.2 is used. The procedure can also be applied to laminates and anisotropic materials. Value of k depends

on ply properties and stacking geometries of the laminate.

In the absence of external load, the total potential energy Π of the strut is expressed as

$$\Pi = \frac{1}{2}\int_0^L EA\varepsilon_x^2 dx + \frac{1}{2}\int_0^L EI\chi_x^2 dx + \frac{1}{2}\int_0^L \frac{GA}{k}\gamma_x^2 dx \qquad (3.1.18)$$

where I is the second moment of area. The three integrands denote the energies due to compression, bending and transverse shear, respectively.

In previous study, Lam (1998) has assumed that the transverse shear effect is negligible. Hence, the transverse shear strain γ_x vanishes in equation (3.1.15). The term χ_x simply becomes $-d^2w/dx^2$ in equation (3.1.14). As a result, only the terms related to compression and bending are included in the potential energy defined in equation (3.1.18) and the energy due to transverse shear is neglected.

3.2 DISPLACEMENT FIELDS AND INITIAL IMPERFECTIONS

In present study, Fourier series and polynomial functions are used to represent the displacement fields and initial imperfections respectively. The representations must satisfy the boundary conditions at the strut ends.

3.2.1 Displacement Fields

When a strut is subjected to applied end-shortening strain ε_o, the displacement u at the strut ends is

$$u = \pm\varepsilon_o \frac{L}{2} \quad \text{at } x = 0, L . \tag{3.2.1}$$

Consistent with the above condition, the displacement field for u is defined as

$$u = \varepsilon_o\left(\frac{L}{2} - x\right) + \sum_i u_i \sin\frac{i\pi x}{L} \tag{3.2.2}$$

where i is an integer and u_i are the unknowns to be determined.

For the out-of-plane simply supported end conditions,

$$w = 0 \text{ and } \beta_x \neq 0 \quad \text{at } x = 0, L . \tag{3.2.3}$$

The displacement fields for w and β_x are

$$w = \sum_i w_i \sin\frac{i\pi x}{L} \tag{3.2.4}$$

$$\beta_x = \sum_i \beta_i \cos\frac{i\pi x}{L} \tag{3.2.5}$$

where w_i and β_i are the unknowns to be determined.

In the finite element method, equal order piecewise polynomial functions are used to simulate the lateral displacement w and rotation β_x. However, when thin material is used, the shear locking effect may thus occur due to the existence of excessive constraint in the limiting case of zero transverse shear strain. Suppose

$$w = \sum_{i=0}^{n} w_i^* x^i \qquad \beta_x = \sum_{i=0}^{n} \beta_i^* x^i \tag{3.2.6}$$

In the limiting case,

$$\gamma_x = \beta_x + \frac{dw}{dx} \rightarrow 0 \qquad (3.2.7)$$

$$\gamma_x = \beta_n^* x^n + \sum_{i=0}^{n-1} [\,[\beta_i^* + (i+1)\, w_i^*]\, x^i\,] \rightarrow 0 \qquad (3.2.8)$$

$$\beta_n^* \rightarrow 0 \qquad (3.2.9)$$

Equation (3.2.9) has demonstrated that the polynomial order of β_x is reduced, because of the different orders in the representations of w and $d\beta_x/dx$. Several numerical techniques have been proposed to alleviate the shear locking effect. Reduced integration was proposed by Zienkiewicz, Taylor and Too (1971). It is a technique commonly used by Prathap and Bhashyam (1982). The element stiffness matrices are no longer evaluated exactly when the order of numerical integration is reduced. Besides, the mixed formulation proposed by Lee and Pian (1978), hybrid formulation developed by Pian (1978) and the field consistency theory proposed by Prathap and Babu (1986) can also be applied to alleviate the shear locking effect, when shear flexible elements are used in thin walled applications.

In the present approach, the use of Fourier series representations is also able to eliminate the shear locking effect. Here,

$$\gamma_x = \sum_i \left[(\beta_i + \frac{i\pi}{L} w_i) \cos \frac{i\pi x}{L} \right] \rightarrow 0 \qquad (3.2.10)$$

A simple relation is established, $\beta_i = -i\pi/L\ w_i$, and in general β_i and w_i are non-zero. Hence, the displacement coefficients defined in equations (3.2.4) and (3.2.5) do not vanish when thin material is used.

3.2.2 General Initial Imperfections

In order to simulate the initial imperfection of a strut, various types of approximate functions can be used, depending on its actual shape. In previous study, Timoshenko and Gere (1961), Yamaki (1959), Shen and William (1995) and Dawe, Wang and Lam (1995) have chosen Fourier series to represent the initial imperfection. In the present approach, the initial imperfection is simulated by a polynomial of degree n and with constant coefficients $a_0, a_1, a_2, \ldots, a_n$, as shown in equation (3.2.11).

$$w_o(x) \cong f(x) = \sum_{j=0}^{n} a_j x^j \qquad (3.2.11)$$

A least-squares technique is applied to match the actual initial imperfection.

$$D = \int (w_o(x) - f(x))^2 dx \qquad (3.2.12)$$

$$D = \sum_{k} (w_o(x_k) - f(x_k))^2 \qquad (3.2.13)$$

The approximate function $f(x)$ is obtained by minimizing the sum of square differences D. Details for determining the coefficients $a_0, a_1, a_2, \ldots, a_n$ can be found in Appendix A. The mathematical expressions shown in equations (3.2.12) and (3.2.13) are the sum of square differences between the actual imperfection $w_o(x)$ and approximate polynomial $f(x)$. The expression in equation (3.2.12) is applied when the initial imperfection is expressed as a well-defined function. For the expression in equation (3.2.13), the magnitudes of initial imperfection are given only at some discrete

points, $x = x_k$ for $k = 1,\ldots,n$, for example, from field measurements of the actual structure.

Other approximations can also be applied to represent the initial imperfection when expressed as a known function. Equation (3.1.13) has shown that the effect of w_o is expressed in terms of dw_o/dx or the slope. It is reasonable to determine the approximate function by simulating the slope along the length of strut.

$$\frac{df(x)}{dx} = \sum_{j=1}^{n} j a_j x^{j-1} \tag{3.2.14}$$

$$D_{slope} = \int \left(\frac{dw_o(x)}{dx} - \frac{df(x)}{dx} \right)^2 dx \tag{3.2.15}$$

Similar least-squares technique, as shown in equation (3.2.15), is used. Again, $f(x)$ is obtained by minimizing D_{slope}. D_{slope} is the sum of square differences between the actual and approximate slope of the initial imperfection.

3.3 SOLUTION PROCEDURES

With the assumption that the strut is homogeneous and prismatic, the values of EA, EI and GA/k are constants throughout the length. Using the displacement fields in equations (3.2.2), (3.2.4) and (3.2.5), Π can be discretized in terms of u_i, w_j and β_m, as shown in equation (3.3.1),

$$\begin{aligned} \Pi = {} & \frac{EA}{L} \varepsilon_o^{\,2} L - \varepsilon_o V_i w_i \\ & + \frac{1}{2} A_{ij}^{(1)} u_i^{\,2} + A_{ij}^{(2)} u_i w_j + \frac{1}{2} A_{ij}^{(3)} w_i w_j + A_{jm}^{(4)} w_j \beta_m + \frac{1}{2} A_{mm}^{(5)} \beta_m^{\,2} \\ & + \frac{1}{2} B_{ijm} u_i w_j w_m + \frac{1}{2} C_{ijm} w_i w_j w_m + \frac{1}{2} D_{ijmn} w_i w_j w_m w_n \end{aligned} \tag{3.3.1}$$

Coefficients of this energy equation are defined as

$$V_i = \frac{EA\pi i}{L}\int_0^L \frac{df(x)}{dx}\cos\frac{i\pi x}{L}\,dx \tag{3.3.2}$$

$$A_{ii}^{(1)} = \delta_{ij}\frac{EA\pi^2 ij}{2L} \tag{3.3.3}$$

$$A_{ij}^{(2)} = EAij\left(\frac{\pi}{L}\right)^2\int_0^L \frac{df(x)}{dx}\cos\frac{i\pi x}{L}\cos\frac{j\pi x}{L}\,dx \tag{3.3.4}$$

$$A_{ij}^{(3)} = EAij\left(\frac{\pi}{L}\right)^2\int_0^L \left(\frac{df(x)}{dx}\right)^2\cos\frac{i\pi x}{L}\cos\frac{j\pi x}{L}\,dx + \delta_{ij}\frac{\pi^2 i^2}{2L}\left(\frac{GA}{k} - \varepsilon_o EA\right) \tag{3.3.5}$$

$$A_{ij}^{(4)} = \delta_{ij}\frac{GA\pi i}{2k} \tag{3.3.6}$$

$$A_{ij}^{(5)} = \delta_{ij}\left(\frac{EI\pi^2 i^2}{2L} + \frac{GAL}{2k}\right) \tag{3.3.7}$$

$$B_{ijm} = EAijk\left(\frac{\pi}{L}\right)^3\int_0^L \cos\frac{i\pi x}{L}\cos\frac{j\pi x}{L}\cos\frac{m\pi x}{L}\,dx \tag{3.3.8}$$

$$C_{ijm} = EAijk\left(\frac{\pi}{L}\right)^3\int_0^L \frac{df(x)}{dx}\cos\frac{i\pi x}{L}\cos\frac{j\pi x}{L}\cos\frac{m\pi x}{L}\,dx \tag{3.3.9}$$

$$D_{ijmn} = \frac{EAijmn}{4}\left(\frac{\pi}{L}\right)^4\int_0^L \cos\frac{i\pi x}{L}\cos\frac{j\pi x}{L}\cos\frac{m\pi x}{L}\cos\frac{n\pi x}{L}\,dx \tag{3.3.10}$$

where δ_{ij} is Kronecker delta.

V_i is the load term due to the end-shortening strain ε_o, $A_{ij}^{(p)}$ ($p = 1,\ldots,5$) are the linear coefficients, B_{ijm} represents the coupling between the displacements u and w, arising form the non-linear terms in the axial strain. C_{ijm} and D_{ijmn} are the non-linear terms related to the lateral displacement w.

In this study, all the above integrands are evaluated analytically. For the coefficients V_i, $A_{ij}^{(2)}$, $A_{ij}^{(3)}$, and C_{ijm}, the integrands comprise of polynomial function due to the initial

imperfection, and trigonometric functions due to the displacement fields. Exact integration is obtained by using the following reduction formula.

$$I_s^{(n)} = \int_0^L x^n \sin ax \, dx = -\frac{L^n}{a}\cos aL + \frac{n}{a} I_c^{(n-1)} \tag{3.3.11}$$

$$I_c^{(n)} = \int_0^L x^n \cos ax \, dx = \frac{L^n}{a}\sin aL - \frac{n}{a} I_s^{(n-1)} \tag{3.3.12}$$

where $a = i\pi/L$. Equations (3.3.11) and (3.3.12) can be easily programmed, and a brief account is given in Chapter 5.

Equilibrium is obtained by applying the principle of minimum potential energy. Three sets of non-linear equations are formed.

$$A_{im}^{(1)} u_m + \left(A_{in}^{(2)} + \frac{1}{2} B_{inp} w_p \right) w_n = 0 \tag{3.3.13}$$

$$\begin{aligned} &- \varepsilon V_j + (A_{mj}^{(2)} + B_{mpj} w_p) u_m \\ &+ \left(A_{jn}^{(3)} + \frac{3}{2} C_{jnp} w_p + 2D_{jnpq} w_p w_q \right) w_n + A_{js}^{(4)} \beta_s = 0 \end{aligned} \tag{3.3.14}$$

$$A_{kn}^{(4)} w_n + A_{ks}^{(5)} \beta_s = 0 \tag{3.3.15}$$

The non-linear problem is solved by the Newton-Raphson method. This set of equilibrium equations is represented in the form of indical notation. In order to express them in matrix form for latter formulation, three column vectors $\{f\}$, $\{g\}$ and $\{h\}$ are introduced to represent the left-hand side of equations (3.3.13), (3.3.14) and (3.3.15) respectively. Here, { } denotes a column vector.

The system of non-linear equilibrium equations (3.3.13) - (3.3.15) is solved by the following iterative procedure.

$$[\boldsymbol{K}^{(i)}] \cdot \{\Delta \boldsymbol{d}^{(i)}\} = -\{\boldsymbol{R}^{(i)}\} \tag{3.3.16}$$

$$\{\boldsymbol{d}^{(i+1)}\} = \{\boldsymbol{d}^{(i)}\} + \{\Delta \boldsymbol{d}^{(i)}\} \tag{3.3.17}$$

where

$$[\boldsymbol{K}^{(i)}] = \begin{bmatrix} \nabla_u \cdot \boldsymbol{f}^{(i)^T} & \nabla_w \cdot \boldsymbol{f}^{(i)^T} & \nabla_\beta \cdot \boldsymbol{f}^{(i)^T} \\ \nabla_u \cdot \boldsymbol{g}^{(i)^T} & \nabla_w \cdot \boldsymbol{g}^{(i)^T} & \nabla_\beta \cdot \boldsymbol{g}^{(i)^T} \\ \nabla_u \cdot \boldsymbol{h}^{(i)^T} & \nabla_w \cdot \boldsymbol{h}^{(i)^T} & \nabla_\beta \cdot \boldsymbol{h}^{(i)^T} \end{bmatrix} \tag{3.3.18}$$

$$\{\nabla_u\} = \left\{\frac{\partial}{\partial u_i}\right\},\ \{\nabla_w\} = \left\{\frac{\partial}{\partial w_j}\right\} \text{ and } \{\nabla_\beta\} = \left\{\frac{\partial}{\partial \beta_m}\right\} \tag{3.3.19}$$

$$\{\boldsymbol{R}^{(i)}\} = \left\lfloor -\boldsymbol{f}^{(i)}, -\boldsymbol{g}^{(i)}, -\boldsymbol{h}^{(i)} \right\rfloor^T \tag{3.3.20}$$

$$\{\boldsymbol{d}^{(i)}\} = \left\lfloor \boldsymbol{u}^{(i)}, \boldsymbol{w}^{(i)}, \boldsymbol{\beta}^{(i)} \right\rfloor^T \tag{3.3.21}$$

$$\frac{\partial f_i}{\partial u_p} = A_{ip}^{(1)}; \qquad \frac{\partial f_i}{\partial w_q} = A_{iq}^{(2)} + B_{iqj} w_j; \qquad \frac{\partial f_i}{\partial \beta_p} = 0 \tag{3.3.22}$$

$$\frac{\partial g_j}{\partial u_p} = A_{jp}^{(2)} + B_{jpq} w_q; \qquad \frac{\partial g_j}{\partial \beta_s} = A_{js}^{(4)} \tag{3.3.23}$$

$$\frac{\partial g_j}{\partial w_q} = A_{jq}^{(3)} + B_{ijq} u_i + 3C_{jqk} w_k + 6D_{jqkl} w_k w_l \tag{3.3.24}$$

$$\frac{\partial h_m}{\partial u_p} = 0; \qquad \frac{\partial h_m}{\partial w_q} = A_{mq}^{(4)}; \qquad \frac{\partial h_m}{\partial \beta_s} = A_{ms}^{(5)} \tag{3.3.25}$$

where $\lfloor\ \rfloor$ denotes a row vector and [ ] denotes a rectangular or square matrix. u_i, w_j and β_k are the coefficients in the displacement fields.

After solving equation (3.3.16), the improvement vector $\{\Delta \boldsymbol{d}^{(i)}\}$ can be obtained. $\{\boldsymbol{d}^{(i+1)}\}$ denotes the improved displacement vector after the i-th iteration, $i = 1, 2, \ldots$. $\{\boldsymbol{d}^{(1)}\}$ is the initial guess. $\{\boldsymbol{f}^{(i)}\}$, $\{\boldsymbol{g}^{(i)}\}$, $\{\boldsymbol{h}^{(i)}\}$, $\{\boldsymbol{R}^{(i)}\}$ and $[\boldsymbol{K}^{(i)}]$ are evaluated at the value $\{\boldsymbol{d}^{(i)}\}$.

The iterative procedures are repeated until the following convergence criterion is satisfied.

$$\frac{\left\|\Delta \boldsymbol{d}^{(i)}\right\|_2}{\left\|\boldsymbol{d}^{(i)}\right\|_2} \leq \tau \qquad (3.3.26)$$

where τ is the tolerance and $\|\boldsymbol{d}\|_2$ is the l_2-norm of vector $\{\boldsymbol{d}\}$. In this study, the tolerance τ is set to be 0.0005.

When $\{\boldsymbol{d}\}$ converges, the displacements u, w and β_x at any point along the strut can be obtained by using the displacement fields introduced in Chapter 3.2. The deformed shape can be traced easily. The average strain ε_{ave} and the average force F_x over the length of the strut are determined by using the equations (3.3.27) and (3.3.28) respectively.

$$\varepsilon_{ave} = \frac{1}{L}\int_0^L \varepsilon_x dx \qquad (3.3.27)$$

$$F_x = EA\varepsilon_{ave} \qquad (3.3.28)$$

Similarly, stress in the x direction $\sigma_x(x,z)$ can also be calculated by substituting the appropriate equations into equation (3.1.16).

In previous study by Lam (1998) without the transverse shear effect, equation (3.3.16) is reduced such that only u_i and w_j are included. The coefficient $A_{ij}^{(3)}$ is redefined as

$$\begin{aligned} A_{ij}^{(3)} = {} & EAij\left(\frac{\pi}{L}\right)^2 \int_0^L \left(\frac{df(x)}{dx}\right)^2 \cos\frac{i\pi x}{L}\cos\frac{j\pi x}{L}\,dx \\ & + \delta_{ij}\left(EI\,\frac{(i\pi)^4}{2L^3} - \varepsilon_0 EA\,\frac{\pi^2 i^2}{2L}\right) \end{aligned} \qquad (3.3.29)$$

Also, Coefficients $A_{ij}^{(4)}$, $A_{ij}^{(5)}$ are neglected in the classical approach.

3.4 APPLICATIONS

Two applications with different initial imperfections are considered. The first one is symmetric and in form of a half sine wave. Comparison is made of the initial imperfections expressed in different forms. Various magnitudes of the imperfections are also considered to indicate the effect.

The other initial imperfection is non-symmetric and in an arbitrary form. Solutions are compared with experiment measurements, which has been provided in previous literature by Lam (1998). Various thickness are considered to verify the transverse shear effect.

3.4.1 Struts with Symmetric Initial Imperfections

The material properties of the strut are EA = 42 N, EI = 504 N mm^2, GA = 15.75 N, L = 600 mm and ν = 1/3. Both ends of the strut are simply supported and a progressive end-shortening is applied. Initial imperfection is symmetric and in the form of a single half sine wave, as shown below.

$$w_o = w_{oh} \sin \frac{\pi x}{L} \tag{3.4.1}$$

w_{oh} is the magnitude of the initial imperfection. Following the procedures described in Chapter 3.2.2, the initial imperfection is simulated by polynomial functions. Equations (3.4.2) - (3.4.6) show the corresponding polynomial expressions with various orders, namely from second to sixth degree respectively.

$$f(\xi) = w_{oh}(3.921\xi - 3.954\xi^2) \quad (3.4.2)$$

$$f(\xi) = w_{oh}(3.744\xi - 3.366\xi^2 - 0.422\xi^3) \quad (3.4.3)$$

$$f(\xi) = w_{oh}(3.103\xi + 0.482\xi^2 - 7.175\xi^3 + 3.591\xi^4) \quad (3.4.4)$$

$$f(\xi) = w_{oh}(3.110\xi + 0.415\xi^2 - 6.973\xi^3 + 3.349\xi^4 + 0.101\xi^5) \quad (3.4.5)$$

$$f(\xi) = w_{oh}(3.142\xi - 0.018\xi^2 - 5.024\xi^3 - 0.550\xi^4 + 3.675\xi^5 - 1.225\xi^6) \quad (3.4.6)$$

where $\xi = x/L$. With the incorporation of constraints for simply supported ends, the constant terms are set to be zero.

Using the criterion of equation (3.2.15), equations (3.4.7) - (3.4.11) show the approximate polynomial functions, for the slope of initial imperfection along the length of strut, of second to sixth order respectively. The sum of square differences between the actual initial imperfection and each polynomial is shown in Table 3.1.

$$f(\xi) = w_{oh}(3.820\xi - 3.820\xi^2) \quad (3.4.7)$$

$$f(\xi) = w_{oh}(3.820\xi - 3.820\xi^2 - 0.000\xi^3) \quad (3.4.8)$$

$$f(\xi) = w_{oh}(3.113\xi + 0.419\xi^2 - 7.065\xi^3 + 3.532\xi^4) \quad (3.4.9)$$

$$f(\xi) = w_{oh}(3.113\xi + 0.419\xi^2 - 7.065\xi^3 + 3.532\xi^4 + 0.000\xi^5) \quad (3.4.10)$$

$$f(\xi) = w_{oh}(3.142\xi - 0.014\xi^2 - 5.042\xi^3 - 0.513\xi^4 + 3.641\xi^5 - 1.214\xi^6) \quad (3.4.11)$$

Table 3.1 Sums of square differences between the actual initial imperfection and approximate polynomials of various orders

Polynomial Order	Approximate by equation (3.2.11), magnitude		Approximate by equation (3.2.15), slope	
	D ($\times w_{oh}$)	D_{slope} ($\times w_{oh}$)	D ($\times w_{oh}$)	D_{slope} ($\times w_{oh}$)
2	5.8101E-04	7.8554E-02	8.0739E-04	7.1385E-02
3	4.5721E-04	9.9559E-02	8.0739E-04	7.1385E-02
4	2.0547E-07	1.0352E-04	3.2820E-07	7.5920E-06
5	1.8438E-07	1.2759E-04	3.2820E-07	7.5920E-06
6	2.4603E-11	2.9356E-08	4.0275E-11	1.7768E-08

D and D_{slope} denote the differences due to the magnitudes and slopes between the actual and approximate imperfection

It is obvious that the difference is smaller for higher order polynomial. Also, the odd order polynomials do not improve the accuracy very much as the initial imperfection is symmetric. In this example, the forth-order polynomial is used in all subsequent studies.

For isotropic material, it is reasonable to assume that the deformed shape is symmetric and similar to the imperfection. The longitudinal displacement u is largest at both ends and is equals to zero at the mid-point. Similar condition can also be applied to the rotation β_x. For displacement w, the maximum value is at the mid-point and is restrained at both ends of the strut. Consistent with the above conditions and the displacement fields defined in Chapter 3.2.1, it is reasonable to assume the following series representations: the first three even sine terms for u, first three odd sine terms for w and first three odd cosine terms for β_x, i.e. sin 2,4,6, sin 1,3,5 and cos 1,3,5 for u, w and β_x respectively.

The magnitude of initial imperfection is first chosen to be w_{oh} = 1 mm. Figures 3.3 and 3.4 show the variations of average strain ε_{ave} with the end-shortening strain ε_o and central deflection $w(A/2) + w_o(A/2)$, respectively. Solutions with initial imperfection

expressed by its exact form are also shown in the figures.

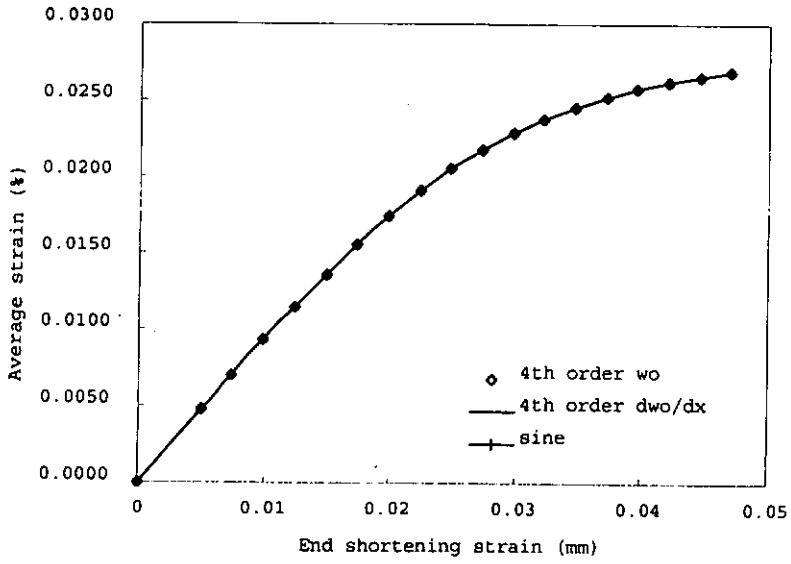

Figure 3.3 Strut with symmetric initial imperfection w_{oh} = 1.0 mm: variation of average strain with end-shortening strain

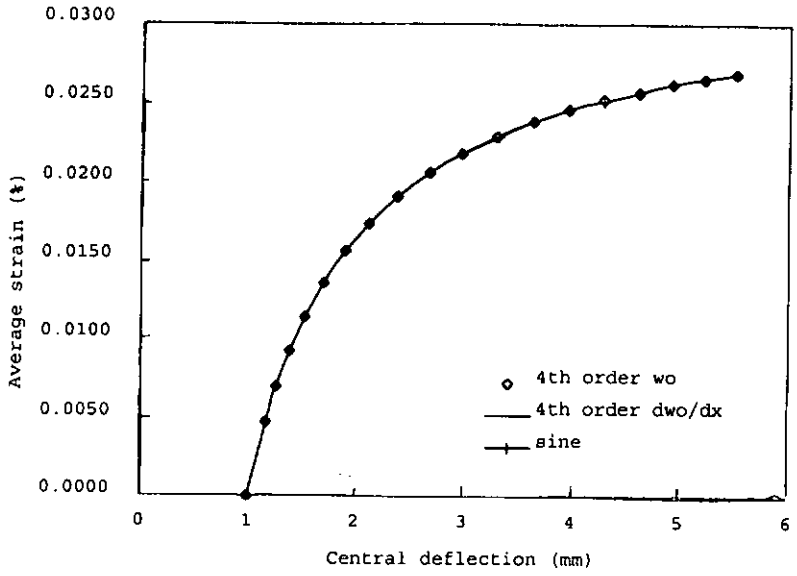

Figure 3.4 Strut with symmetric initial imperfection w_{oh} = 1.0 mm: variation of average strain with central deflection

From the figures, very close comparisons are obtained for results predicted with the initial imperfections expressed in the

exact form or in both approximate functions. It shows the adaptability of using the present approaches, by magnitude and by slope, to simulate the actual initial imperfection.

In the next study, the magnitude of initial imperfection is increased to 2.5 mm. Similar analysis is performed to demonstrate the effect of the magnitude of imperfection.

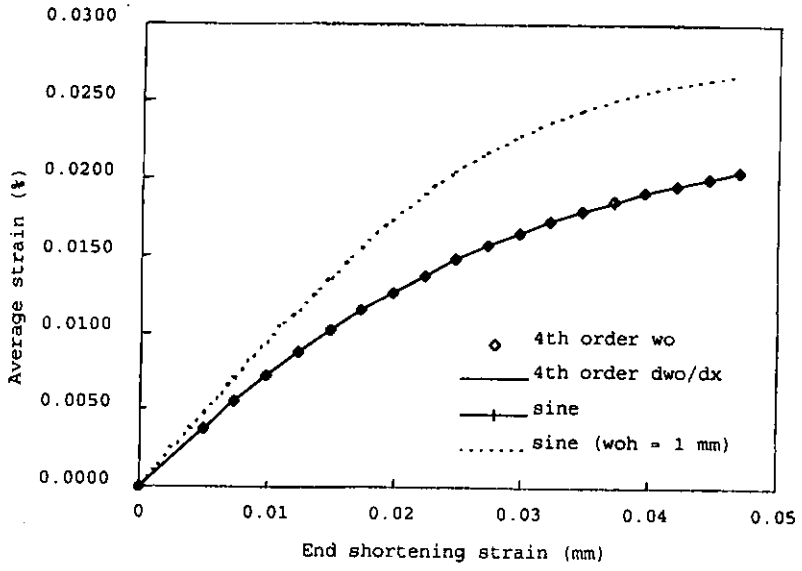

Figure 3.5 Strut with symmetric initial imperfection w_{oh} = 2.5 mm: variation of average strain with end-shortening strain

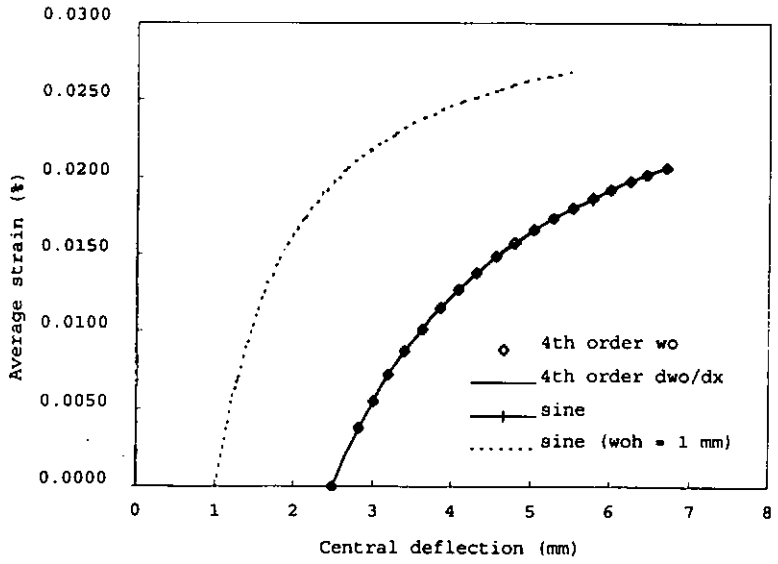

Figure 3.6 Strut with symmetric initial imperfection w_{oh} = 2.5 mm: variation of average strain with central deflection

Results obtained by both approximate imperfections are also in good agreements. Figure 3.5 shows that less force is required under a progressive end-shortening strain, as compared with the previous case having w_{oh} = 1.0 mm. Reason of this phenomenon is that the bending effect becomes more significant when the magnitude of imperfection increases. Variation of average strain with central deflection is shown in Figure 3.6.

3.4.2 Struts with Non-Symmetric Initial Imperfection

In this example, the strut has a non-symmetric initial imperfection. A forth-order polynomial, as shown in equation (3.4.12), is used to simulate the actual shape. Table 3.2 compares the actual and approximate values of initial imperfection.

$$f(\xi) = 8.1295\xi + 15.0753\xi^2 - 41.8137\xi^3 + 18.6088\xi^4 \qquad (3.4.12)$$

where $\xi = x/L$.

Table 3.2 Comparison of actual shape of the initial imperfection with the corresponding approximate function

	w_o (mm)	
ξ	Actual	Approximate
0.0	0.00	0.00
0.1	0.81	0.93
0.2	1.98	1.92
0.3	2.87	2.82
0.4	3.46	3.46
0.5	3.75	3.77
0.6	3.64	3.69
0.7	3.23	3.20
0.8	2.36	2.37
0.9	1.28	1.26
1.0	0.00	0.00

The strut is made from an aluminum strip with modulus of elasticity E = 71 kN/mm^2. It is 600 mm long with a uniform cross-section of 25 mm wide and 3 mm thick. Ends of the strut are simply supported. Experimental measurements and analysis with no transverse shear effect of the same problem have been given by Lam (1998).

Since the initial imperfection is non-symmetric, trigonometric series representations with sin 1-5, sin 1-10 and cos 1-10 are used for the displacement fields u, w and β_x respectively. When the progressive end-shortening strain is applied, the strut deforms laterally. Deflections obtained from experimental measurements and analysis results are recorded in Table 3.3. Figure 3.7 shows the deformed shapes of the strut at three levels of end-shortening strain. The total deflections $w_o + w$ at three specific points (x = $L/4$, $L/2$ and $3L/4$) are shown in Figure 3.8. The variation of average strain ε_{ave} with the end shorting strain is shown in Figure 3.9.

Table 3.3 Total deflections at three levels of end-shortening strain

	ε_o =0.09%			ε_o =0.13%			ε_o =0.1617%		
ξ	Exp't	no sh'r	shear	Exp't	no sh'r	shear	Exp't	no sh'r	shear
0.250	8.49	8.15	8.15	10.33	9.72	9.72	11.53	10.81	10.81
0.375	11.13	10.91	10.91	13.53	12.96	12.96	15.09	14.38	14.39
0.500	12.28	12.01	12.01	14.87	14.24	14.24	16.65	15.78	15.79
0.625	11.41	11.24	11.24	13.81	13.30	13.30	15.38	14.72	14.73
0.750	8.81	8.69	8.69	10.65	10.27	10.27	11.84	11.36	11.36

Exp't: Experiment; no sh'r: analysis without transverse shear effect; shear: analysis with transverse shear effect

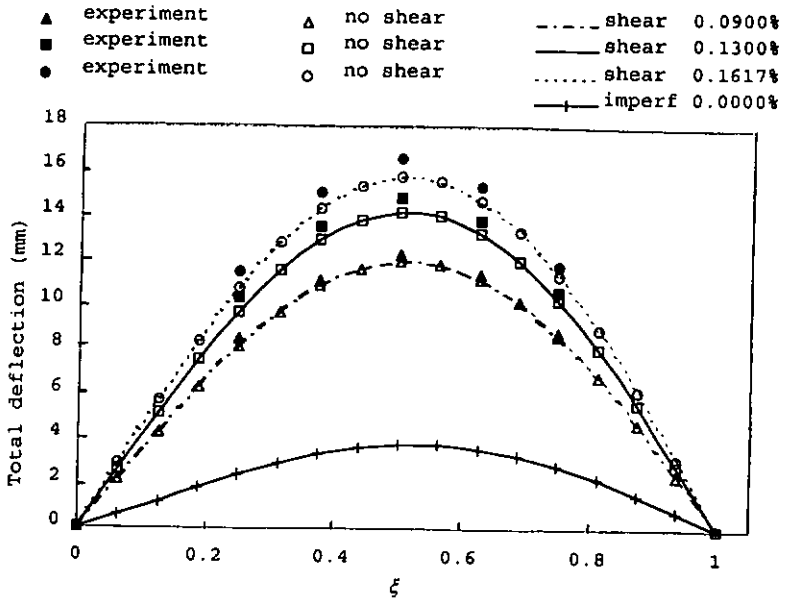

Figure 3.7 Strut with general initial imperfection: deformed shapes at three levels of end-shortening strain

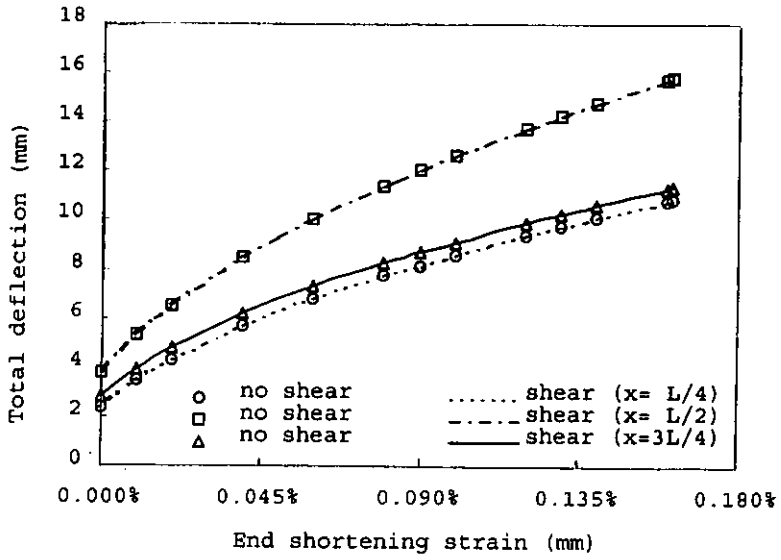

Figure 3.8 Strut with general initial imperfection: variation of total deflection (at $x = L/4,\ L/2,\ 3L/4$) with end-shortening strain

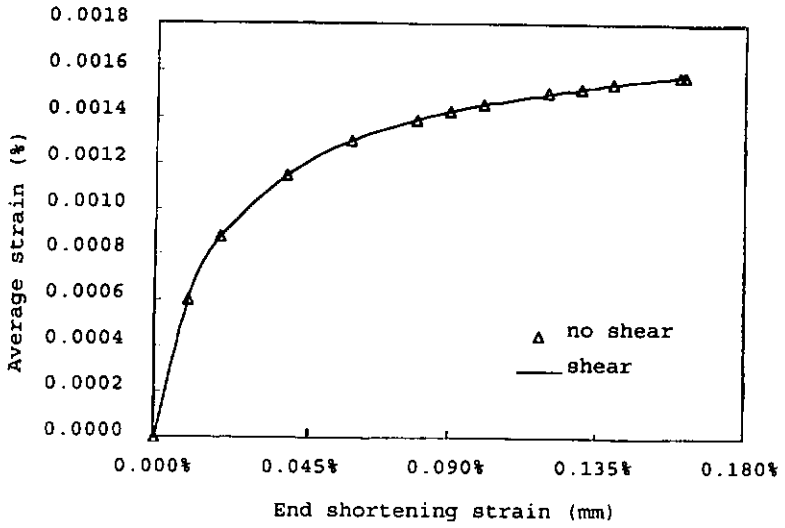

Figure 3.9 Strut with general initial imperfection: variation of average strain with end-shortening strain

Although the initial imperfection is non-symmetric, the deformed shape of the strut as shown in Figure 3.7 tends to be in a single half sine wave at high level of strain. From the above table and figures, the results obtained by using the present approach (with transverse shear effect) are in good agreement with experimental

measurements and are almost the same as the solution obtained from the analysis with no consideration of the transverse shear effect.

An application with a thickness h = 30 mm is then considered. Other material properties are the same as the previous case. Both analyses with or without the transverse shear effect are performed using the same series representations for u, w and β_x.

Figure 3.10 shows the relation of the average strain and the end-shortening strain for the strut with h = 30. It is noted that a larger axial load $F_x = EA\,\varepsilon_{ave}$ is required to achieve similar end-shortening strain as compared with a thinner strut.

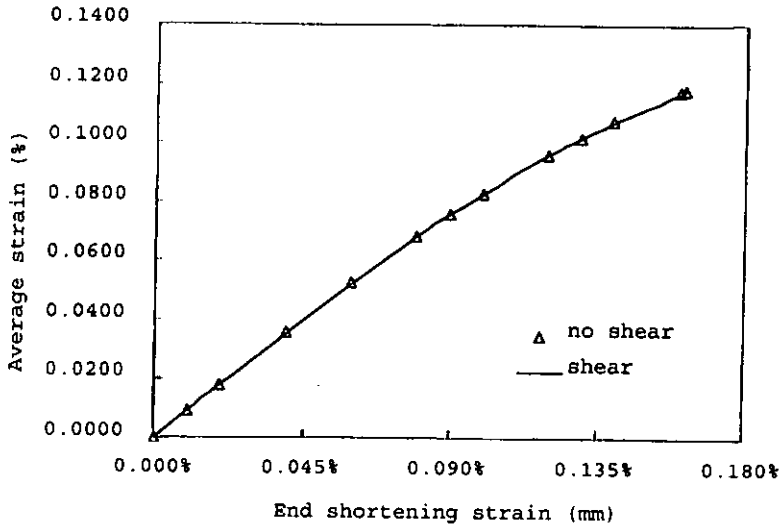

Figure 3.10 Strut with general initial imperfection (h = 30): variation of average strain with end-shortening strain

Table 3.4 Total deflections of strut with thickness h = 30 at three levels of end-shortening strain

	ε_o =0.09%		ε_o =0.13%		ε_o =0.1617%	
ξ	no sh'r	shear	no sh'r	shear	no sh'r	shear
0.250	3.90	3.92	4.95	4.97	5.93	5.95
0.375	5.32	5.34	6.70	6.73	7.98	8.01
0.500	5.94	5.96	7.44	7.47	8.83	8.86
0.625	5.62	5.64	7.01	7.04	8.30	8.33
0.750	4.38	4.39	5.45	5.47	6.43	6.46

In Table 3.4, smaller deflections are observed when the thickness of strut changes from 3 mm to 30 mm. The differences between the analyses with and without transverse shear effect become larger. According to Table 3.3 (for h = 3 mm), the percentage differences with respect to the results with shear effect are below 0.08% at all points along the length of strut and at all levels of end-shortening strain below 0.1617%. However, the differences increase to about 0.28% at ε_o = 0.09%, 0.37% at ε_o = 0.13% and 0.40% at ε_o = 0.1617%, while the thickness is 30 mm.

Convergence is one of the most important considerations for an efficient analytical approach. In solving the non-linear problem, an iterative approach, Newton-Raphson method, is employed. Table 3.5 shows the number of iterations for each increment of end-shortening strain in the analyses of both thickness. Excellent rates of convergence have be recorded. Not more than seven and four iterations are required for all twelve increments in the analyses of h = 3 mm and h = 30 mm, respectively.

Table 3.5 Number of iterations for each increment of end-shortening strain in the analyses of thickness h = 3 mm and h = 30 mm

Increment	ε_o	No. of iterations	
		h = 3 mm	h = 30 mm
1	0.0100%	7	3
2	0.0200%	5	3
3	0.0400%	6	3
4	0.0600%	5	3
5	0.0800%	5	3
6	0.0900%	4	3
7	0.1000%	4	3
8	0.1200%	4	4
9	0.1300%	4	3
10	0.1400%	4	3
11	0.1600%	4	4
12	0.1617%	2	3

To conclude, the present approach is applicable to the post-buckling analysis of strut with general initial imperfection. Excellent rate of convergence is observed using the Newton-Raphson method. The included transverse shear effect shows an accurate prediction when the thickness of strut increase (or L/h is smaller). On the other hand, the present approach is also adaptable when the thickness decreases. The shear locking effect is alleviated in the limiting condition of thin strut (or large value of L/h) because of the use of equal terms Fourier series to represent both the lateral displacement and rotation. As a result, the order of displacement fields is not reduced, as one might expect in the case of polynomial functions, having shear locking effect.

CHAPTER 4

POST-BUCKLING ANALYSIS OF LAMINATED PLATE WITH GENERAL INITIAL IMPERFECTION USING FINITE STRIP METHOD

In Chapter 3, an approach for the post-buckling analysis of a strut is introduced in a manner that the deformation and initial imperfection are represented by Fourier series and polynomial functions respectively. The work is extended and reported in this chapter for the post-buckling analysis of laminated plates with general initial imperfection when subjected to progressive end-shortening. A finite strip approach developed in the context of classical plate theory is extended with the use of appropriate polynomial to simulate the initial imperfection

4.1 LAMINATE EQUATIONS

Figure 4.1 shows a typical finite strip with width b, which forms part of a rectangular laminated plate of length A, width B ($B \geq b$) and thickness h. While the plate is subjected to an in-plane compressive loading, a uniform end-shortening strain ε_0 occurs along the edges parallel to the y-axis (the ends of finite strips). Two alternatives of lateral expansion at the loaded ends are considered. Such an expansion can be either free or completely prevented. The strip ends are assumed to be simply supported out-of-plane. Boundary conditions for in-plane and out-of-plane deformations along the unloaded edges (parallel to the x-axis) are specified by imposing restraints on the nodal unknowns along these edges. Details on the classification of the boundary conditions can

be found in the reference by Chia (1980).

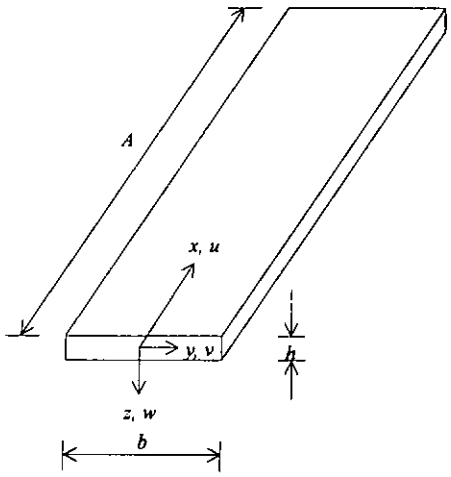

Figure 4.1 A typical finite strip

Applying the classical plate theory by incorporating Kirchhoff normalcy condition, the three fundamental components of displacement at a general point $(\bar{u}, \bar{v}, \bar{w})$ can be expressed as

$$\bar{u}(x, y, z) = u(x, y) - z \frac{\partial w(x, y)}{\partial x} \tag{4.1.1}$$

$$\bar{v}(x, y, z) = v(x, y) - z \frac{\partial w(x, y)}{\partial y} \tag{4.1.2}$$

$$\bar{w}(x, y, z) = w(x, y) \tag{4.1.3}$$

where u, v and w are the displacements on the middle surface in the x, y and z directions respectively.

Consistent with the von Karman assumptions, for instance see Novozhilov (1953), the in-plane strain $\{\varepsilon\}$ with respect to the displacements at a general point is defined as

$$\{\varepsilon\} = \{\varepsilon_L\} + \{\varepsilon_{NL}\} + \{\varepsilon_I\} \tag{4.1.4}$$

$$\{\varepsilon_L\} = \begin{Bmatrix} \dfrac{\partial u}{\partial x} \\ \dfrac{\partial v}{\partial y} \\ \dfrac{\partial u}{\partial y} + \dfrac{\partial v}{\partial x} \end{Bmatrix} \quad \{\varepsilon_{NL}\} = \begin{Bmatrix} \dfrac{1}{2}\left(\dfrac{\partial w}{\partial x}\right)^2 \\ \dfrac{1}{2}\left(\dfrac{\partial w}{\partial y}\right)^2 \\ \dfrac{\partial w}{\partial x}\dfrac{\partial w}{\partial y} \end{Bmatrix} \quad \{\varepsilon_I\} = \begin{Bmatrix} \dfrac{\partial w_o}{\partial x}\dfrac{\partial w}{\partial x} \\ \dfrac{\partial w_o}{\partial y}\dfrac{\partial w}{\partial y} \\ \dfrac{\partial w_o}{\partial x}\dfrac{\partial w}{\partial y} + \dfrac{\partial w_o}{\partial y}\dfrac{\partial w}{\partial x} \end{Bmatrix} \tag{4.1.5}$$

The in-plane strain $\{\varepsilon\}$ consists of three components. $\{\varepsilon_L\}$ and $\{\varepsilon_{NL}\}$ are the strain components involving linear and non-linear displacements respectively, and $\{\varepsilon_I\}$ includes the effect of initial imperfection w_o.

The bending strains $\{\chi\}$ and end-shortening strains $\{e\}$ are defined in equation (4.1.6).

$$\{\chi\} = \begin{Bmatrix} -\dfrac{\partial^2 w}{\partial x^2} \\ -\dfrac{\partial^2 w}{\partial y^2} \\ -2\dfrac{\partial^2 w}{\partial x \partial y} \end{Bmatrix} \qquad \{e\} = \varepsilon_o \begin{Bmatrix} -1 \\ \alpha \\ 0 \end{Bmatrix} \tag{4.1.6}$$

ε_o is the prescribed uniform end-shortening strain. α is a constant which may or may not be equal to zero, depending on the boundary condition at the loaded ends. A description of α is given in Chapter 4.2.

The constitutive equations, Whitney (1987), for a plate are obtained through the use of stress-strain relations and appropriate integration through the uniform thickness h.

$$\begin{Bmatrix} N \\ M \end{Bmatrix} = \begin{bmatrix} A & B \\ B & D \end{bmatrix} \begin{Bmatrix} e + \varepsilon \\ \chi \end{Bmatrix} \tag{4.1.7}$$

where

$$\{N\} = \begin{Bmatrix} N_x \\ N_y \\ N_{xy} \end{Bmatrix} = \int_{-h/2}^{h/2} \begin{Bmatrix} \sigma_x \\ \sigma_y \\ \tau_{xy} \end{Bmatrix} dz \qquad (4.1.8)$$

$$\{M\} = \begin{Bmatrix} M_x \\ M_y \\ M_{xy} \end{Bmatrix} = \int_{-h/2}^{h/2} \begin{Bmatrix} z\sigma_x \\ z\sigma_y \\ z\tau_{xy} \end{Bmatrix} dz \qquad (4.1.9)$$

$$\begin{Bmatrix} A_{ij} \\ B_{ij} \\ D_{ij} \end{Bmatrix} = \int_{-h/2}^{h/2} Q_{ij} \begin{Bmatrix} 1 \\ z \\ z^2 \end{Bmatrix} dz \qquad i, j = 1, 2, 6 \qquad (4.1.10)$$

$\{N\}$ comprises the direct and shearing stress resultants per unit length and $\{M\}$ consists of the bending and twisting stress couples per unit length. Q_{ij} are plane-stress stiffness coefficients.

Table 4.1 Summary of coefficients A_{ij}, B_{ij} and D_{ij} in various materials

	$[A]$	$[B]$	$[D]$
Isotropic	$\begin{bmatrix} A_{11} & A_{12} & 0 \\ A_{12} & A_{11} & 0 \\ 0 & 0 & A_{66} \end{bmatrix}$	$\begin{bmatrix} 0 & 0 & 0 \\ 0 & 0 & 0 \\ 0 & 0 & 0 \end{bmatrix}$	$\begin{bmatrix} D_{11} & D_{12} & 0 \\ D_{12} & D_{11} & 0 \\ 0 & 0 & D_{66} \end{bmatrix}$
Symmetric Cross-Ply	$\begin{bmatrix} A_{11} & A_{12} & 0 \\ A_{12} & A_{11} & 0 \\ 0 & 0 & A_{66} \end{bmatrix}$	$\begin{bmatrix} 0 & 0 & 0 \\ 0 & 0 & 0 \\ 0 & 0 & 0 \end{bmatrix}$	$\begin{bmatrix} D_{11} & D_{12} & 0 \\ D_{12} & D_{11} & 0 \\ 0 & 0 & D_{66} \end{bmatrix}$
Non-Symmetric Cross-Ply $[0°, 90°]_n$	$\begin{bmatrix} A_{11} & A_{12} & 0 \\ A_{12} & A_{11} & 0 \\ 0 & 0 & A_{66} \end{bmatrix}$	$\begin{bmatrix} B_{11} & 0 & 0 \\ 0 & -B_{11} & 0 \\ 0 & 0 & 0 \end{bmatrix}$	$\begin{bmatrix} D_{11} & D_{12} & 0 \\ D_{12} & D_{11} & 0 \\ 0 & 0 & D_{66} \end{bmatrix}$
Symmetric Angle-Ply	$\begin{bmatrix} A_{11} & A_{12} & 0 \\ A_{12} & A_{22} & 0 \\ 0 & 0 & A_{66} \end{bmatrix}$	$\begin{bmatrix} 0 & 0 & 0 \\ 0 & 0 & 0 \\ 0 & 0 & 0 \end{bmatrix}$	$\begin{bmatrix} D_{11} & D_{12} & 0 \\ D_{12} & D_{22} & 0 \\ 0 & 0 & D_{66} \end{bmatrix}$
Non-Symmetric Angle-Ply $[+\theta, -\theta]_n$	$\begin{bmatrix} A_{11} & A_{12} & 0 \\ A_{12} & A_{22} & 0 \\ 0 & 0 & A_{66} \end{bmatrix}$	$\begin{bmatrix} 0 & 0 & B_{16} \\ 0 & 0 & B_{26} \\ B_{16} & B_{26} & 0 \end{bmatrix}$	$\begin{bmatrix} D_{11} & D_{12} & 0 \\ D_{12} & D_{22} & 0 \\ 0 & 0 & D_{66} \end{bmatrix}$

The form of constitutive equations (4.1.7) is very general, which allows anisotropic laminate properties with regard to both in-plane behavior (through the presence of the A_{16} and A_{26} coefficients) and out-of-plane behavior (through the D_{16} and D_{26} coefficients), and full coupling between in-plane and out-of-plane behaviors (through the B_{ij} coefficients). A summary of the coefficients A_{ij}, B_{ij} and D_{ij} for various materials are shown in Table 4.1.

When uniform end-shortening strain is applied in the absence of an external force, the potential energy of a strip can be expressed in the form of

$$\Pi_p = \frac{1}{2}\int\left\{\begin{matrix}\boldsymbol{\varepsilon} + \boldsymbol{e} \\ \boldsymbol{\chi}\end{matrix}\right\}^T \begin{bmatrix}\boldsymbol{A} & \boldsymbol{B} \\ \boldsymbol{B} & \boldsymbol{D}\end{bmatrix} \left\{\begin{matrix}\boldsymbol{\varepsilon} + \boldsymbol{e} \\ \boldsymbol{\chi}\end{matrix}\right\} dxdy \qquad (4.1.12)$$

The effect of in-plane load is indirectly applied through the end-shortening effect, and hence $\{\boldsymbol{\varepsilon} + \boldsymbol{e}\}$ is also expressed in terms of the prescribed end-shortening strain ε_o.

4.2 STRIP DISPLACEMENT FIELDS AND BOUNDARY CONDITIONS

Using the finite strip method, the displacements u, v and w are represented by the following displacement fields

$$u = \varepsilon_o\left(\frac{A}{2} - x\right) + \sum_i U_i(x)g_i^u(y) \qquad (4.2.1)$$

$$v = \alpha\varepsilon_o y + \sum_i V_i(x)g_i^v(y) \qquad (4.2.2)$$

$$w = \sum_i W_i(x)g_i^w(y) \qquad (4.2.3)$$

$g_i^u(y)$, $g_i^v(y)$ and $g_i^w(y)$ are crosswise polynomial interpolation functions of various types and orders, involving undetermined displacement coefficients, u_{im}, v_{im}, w_{im} and ψ_{im}.

$$g_i^u(y) = \sum_m N_m^u(y) u_{im} \tag{4.2.4}$$

$$g_i^v(y) = \sum_m N_m^v(y) v_{im} \tag{4.2.5}$$

$$g_i^w(y) = N_1^w(y) w_{i1} + \hat{N}_1^w(y) \psi_{i1} + N_2^w(y) w_{i2} + \hat{N}_2^w(y) \psi_{i2} \tag{4.2.6}$$

$N(y)$ is the shape function. For the in-plane displacements u and v, Lagrange interpolating polynomials are applied. Dawe, Lam and Azizian (1992) compared the responses of perfect plates by using various orders of polynomial. It has been shown that acceptable accuracy could be obtained when quadratic polynomial has been applied. Thus, the quadratic polynomial is used in this study. For the out-of-plane displacements w and ψ ($\psi = \partial w/\partial y$), cubic Hermite interpolating polynomial is used. Figure 4.2 shows the nodal points on a quadratic strip end. Shape functions for the quadratic finite strip model are given in equations (4.2.7) - (4.2.13).

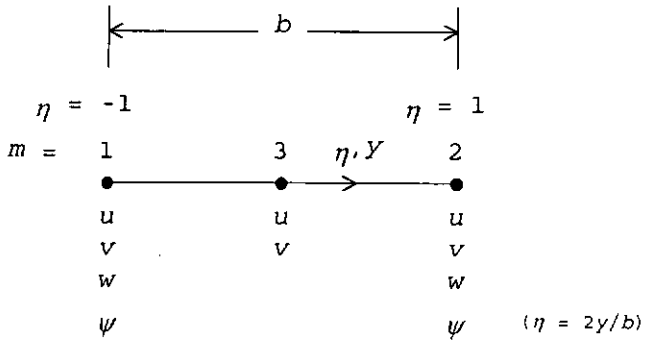

Figure 4.2 Nodal points for u, v, w and ψ on a quadratic strip end

$$N_1^u = N_1^v = \frac{1}{2}(\eta^2 - \eta) \tag{4.2.7}$$

$$N_2^u = N_2^v = \frac{1}{2}(\eta^2 + \eta) \tag{4.2.8}$$

$$N_3^u = N_3^v = 1 - \eta^2 \tag{4.2.9}$$

$$N_1^w = \frac{1}{4}(2 - 3\eta + \eta^3) \tag{4.2.10}$$

$$N_2^w = \frac{1}{4}(2 + 3\eta - \eta^3) \tag{4.2.11}$$

$$\hat{N}_1^w = \frac{b}{8}(1 - \eta - \eta^2 + \eta^3) \tag{4.2.12}$$

$$\hat{N}_2^w = \frac{b}{8}(-1 - \eta + \eta^2 + \eta^3) \tag{4.2.13}$$

$U_i(x)$, $V_i(x)$ and $W_i(x)$ are longitudinal functions satisfying the kinematic conditions prescribed at the strip ends. These functions are series of sine or cosine. The expression for displacement u further involves the prescribed uniform end-shortening strain ε_o at loaded ends. Each strip end is assumed to be simply supported in the out-of-plane direction. The pre-buckling deformation is

$$u = \pm\varepsilon_o \frac{A}{2} \quad \text{at } x = 0, A \tag{4.2.14}$$

Two types of problem are considered according to the lateral expansions along the loaded edges. In Type A problem, the plate is free to expand laterally along the loaded edges. The longitudinal series terms for v are cosine functions, as shown in Table 4.2. The term $\alpha\varepsilon y$ represents the lateral expansion of plate, at x = 0 and A, under uniform compression. The situation applies for isotropic plates (where $\alpha = \nu$) and for orthotropic, symmetrically laminated plates (where $\alpha = A_{12} / A_{22}$). For laminated plates involving anisotropy and coupling in-plane and out-of-plane properties, the

presence of the term $\alpha\varepsilon y$ is irrational. For consistency, this term is retained and is defined as $\alpha = A_{12} / A_{22}$ in the analysis of a full range of plate properties.

In Type B problem, lateral expansions along the loaded edges are restrained completely. Sine functions are used to represent the longitudinal series for v and parameter α is zero.

Table 4.2 Longitudinal functions and parameter satisfying the Type A and Type B conditions

	Type A	Type B
$U_i(x)$	$\sin \frac{i\pi x}{A}$	$\sin \frac{i\pi x}{A}$
$V_i(x)$	$\cos \frac{i\pi x}{A}$ including the term $i = 0$	$\sin \frac{i\pi x}{A}$
$W_i(x)$	$\sin \frac{i\pi x}{A}$	$\sin \frac{i\pi x}{A}$
α	v or A_{12}/A_{22}	0

v is Poisson's ratio

For the in-plane and out-of-plane conditions along the unloaded edges, restraints are imposed directly to the displacement coefficients, u_{im}, v_{im}, w_{im} and ψ_{im}, on the corresponding nodal lines.

4.3 GENERAL INITIAL IMPERFECTION

In this study, plate with small initial imperfection in z direction is allowed. The total deflection w_t normal to the xy plane is

$$w_t = w_o + w \tag{4.3.1}$$

where w_o is the initial imperfection and w is the additional deformation due to the applied loading.

The displacement field for w is defined in Chapter 4.2 and the initial imperfection w_o within a finite strip is expressed as

$$w_o = \sum_i f_i(x) g_i^{wo}(y) \tag{4.3.2}$$

where $f_i(x)$ is the shape of longitudinal initial imperfection along the i-th nodal line in a finite strip and

$$g_i^{wo}(y) = \sum_m N_m^{wo}(y)\, w_{oim} \tag{4.3.3}$$

$g_i^{wo}(y)$ is the crosswise function containing the magnitude of imperfection w_{oim} of each nodal line. Here, $N_m^{wo}(y)$ is the quadratic Lagrange interpolation polynomial, which is the same as the shape functions $N_m^u(y)$ and $N_m^v(y)$ defined in Chapter 4.2.

When simulating the initial imperfection along each longitudinal nodal line, various types of approximate functions can be used. This depends on the actual shape of the initial imperfection. On the assumption that the initial imperfection is in the form of a half sine wave, Fourier series as shown in equation (4.3.4) have been used by Saigal, Kapania and Yang (1986).

$$f_i(x) = \sin \frac{i\pi x}{A} \tag{4.3.4}$$

In this study, polynomial functions are used to simulate the longitudinal shapes of the initial imperfection. Equation (4.3.5)

is the n-order polynomial function along the i-th nodal line in a finite strip.

$$f_i(x) = \sum_{j=0}^{n} a_{ij} x^j \qquad (4.3.5)$$

Coefficients a_{ij} are determined by applying the least-squares technique. Details of the procedure can be found in Appendix A. It is applicable for initial imperfection defined either by exact function or by discrete measurements. This approach is similar to that being applied in simulating the imperfection of strut in Chapter 3.2. However, in this case, the expression for initial imperfection is repeated for each nodal line i.

This approach is suitable for approximating the initial imperfection in very general shape. However, there is a restriction in that measurements of the imperfection must be along each nodal line. As an alternative approximate functions for the whole plate, as shown in equation (4.3.6), can be used instead of equation (4.3.2).

$$w_o = \sum_i \sum_j a_{ij} x^i y^j \qquad (4.3.6)$$

It is able to approximate the initial imperfection no matter where the measurements are being taken. However, accuracy of equation (4.3.6) reduced and a more complicated formulation is required.

4.4 SOLUTION PROCEDURES

With the establishment of the finite strip displacement fields

and initial imperfection described in Chapter 4.2 and 4.3, the strain-displacement relations, defined in equations (4.1.5) and (4.1.6), can be expressed in matrix forms

$$\{\varepsilon_L\} = [B_L]\{d_p\} \quad \{\varepsilon_I\} = [B_I]\{d_b\} \tag{4.4.1}$$

$$\{\varepsilon_{NL}\} = \frac{1}{2}[B_{NL}]\{d_b\} \tag{4.4.2}$$

$$\{e\} = \varepsilon_o\{b_e\} \quad \{\chi\} = [B_\chi]\{d_b\} \tag{4.4.3}$$

where the column vectors, $\{d_p\}$ and $\{d_b\}$, represent the in-plane $\lfloor u_{im}, v_{im} \rfloor^T$ and out-of-plane $\lfloor w_{im}, \psi_{im} \rfloor^T$ unknown displacement coefficients respectively.

$$[B_L] = \begin{bmatrix} \left\lfloor \frac{\partial U_i}{\partial x} N_j^u \right\rfloor & 0 \\ 0 & \left\lfloor V_i \frac{\partial N_j^v}{\partial y} \right\rfloor \\ \left\lfloor U_i \frac{\partial N_j^u}{\partial y} \right\rfloor & \left\lfloor \frac{\partial V_i}{\partial x} N_j^v \right\rfloor \end{bmatrix} \tag{4.4.4}$$

$$[B_I] = \begin{bmatrix} \left\lfloor \frac{\partial w_o}{\partial x} \frac{\partial W_i}{\partial x} N_j^w \right\rfloor & \left\lfloor \frac{\partial w_o}{\partial x} \frac{\partial W_i}{\partial x} \hat{N}_j^w \right\rfloor \\ \left\lfloor \frac{\partial w_o}{\partial y} W_i \frac{\partial N_j^w}{\partial y} \right\rfloor & \left\lfloor \frac{\partial w_o}{\partial y} W_i \frac{\partial \hat{N}_j^w}{\partial y} \right\rfloor \\ \left\lfloor \frac{\partial w_o}{\partial x} W_i \frac{\partial N_j^w}{\partial y} + \frac{\partial w_o}{\partial y} \frac{\partial W_i}{\partial x} N_j^w \right\rfloor & \left\lfloor \frac{\partial w_o}{\partial x} W_i \frac{\partial \hat{N}_j^w}{\partial y} + \frac{\partial w_o}{\partial y} \frac{\partial W_i}{\partial x} \hat{N}_j^w \right\rfloor \end{bmatrix} \tag{4.4.5}$$

$$[B_\chi] = \begin{bmatrix} \left\lfloor -\frac{\partial^2 W_i}{\partial x^2} N_j^w \right\rfloor & \left\lfloor -\frac{\partial^2 W_i}{\partial x^2} \hat{N}_j^w \right\rfloor \\ \left\lfloor -W_i \frac{\partial^2 N_j^w}{\partial y^2} \right\rfloor & \left\lfloor -W_i \frac{\partial^2 \hat{N}_j^w}{\partial y^2} \right\rfloor \\ \left\lfloor -2 \frac{\partial W_i}{\partial x} \frac{\partial N_j^w}{\partial y} \right\rfloor & \left\lfloor -2 \frac{\partial W_i}{\partial x} \frac{\partial \hat{N}_j^w}{\partial y} \right\rfloor \end{bmatrix} \tag{4.4.6}$$

$$[\boldsymbol{B}_{NL}] = [\boldsymbol{C}] \cdot [\boldsymbol{S}] = \begin{bmatrix} \frac{\partial w}{\partial x} & 0 \\ 0 & \frac{\partial w}{\partial y} \\ \frac{\partial w}{\partial y} & \frac{\partial w}{\partial x} \end{bmatrix} \cdot \begin{bmatrix} \left[\frac{\partial W_i}{\partial x} N_j^w\right] & \left[\frac{\partial W_i}{\partial x} \hat{N}_j^w\right] \\ \left[W_i \frac{\partial N_j^w}{\partial y}\right] & \left[W_i \frac{\partial \hat{N}_j^w}{\partial y}\right] \end{bmatrix} \tag{4.4.7}$$

Definition of $\{\boldsymbol{b}_e\}$ has been shown in equation (4.1.6).

Total potential energy Π of the whole plate is simply the summation of all the potential energies Π_p of the individual finite strips. Equilibrium of the plate can be obtained by substituting the strain components in equations (4.4.1) to (4.4.3) into Π and applying the principle of minimum potential energy.

$$\Pi = \sum \Pi_p \tag{4.4.8}$$

$\{\boldsymbol{d}\} = \lfloor \boldsymbol{d}_p, \boldsymbol{d}_b \rfloor^T = \{d_k\}$ is the displacement vector of all displacement coefficients. Newton-Raphson method is applied to solve the non-linear problem, and all the entries d_k are determined by the following iterative procedures.

$$[\boldsymbol{K}_T]\{\Delta \boldsymbol{d}^{(i)}\} = -[\boldsymbol{K}]\{\boldsymbol{d}^{(i)}\} + \varepsilon_0\{\boldsymbol{p}\} \tag{4.4.9}$$

$$\{\boldsymbol{d}^{(i+1)}\} = \{\Delta \boldsymbol{d}^{(i)}\} + \{\boldsymbol{d}^{(i)}\} \tag{4.4.10}$$

where

$$\delta\Pi = \{\delta \boldsymbol{d}\}^T([\boldsymbol{K}]\{\boldsymbol{d}\} - \varepsilon_0\{\boldsymbol{p}\}) \qquad \delta^2\Pi = \{\delta \boldsymbol{d}\}^T[\boldsymbol{K}_T]\{\delta \boldsymbol{d}\} \tag{4.4.11}$$

$$[\boldsymbol{K}_T] = [\boldsymbol{K}_L] + [\boldsymbol{K}_{NL}] + [\boldsymbol{K}_Q] \tag{4.4.12}$$

$$[\boldsymbol{K}] = [\boldsymbol{K}_L] + [\boldsymbol{K}_{NL2}] \tag{4.4.13}$$

$$[\boldsymbol{K}_L] = \int \begin{bmatrix} \boldsymbol{B}_L^T \boldsymbol{A} \boldsymbol{B}_L & \boldsymbol{B}_L^T \boldsymbol{A} \boldsymbol{B}_I + \boldsymbol{B}_L^T \boldsymbol{B} \boldsymbol{B}_\chi \\ \boldsymbol{B}_I^T \boldsymbol{A} \boldsymbol{B}_L + \boldsymbol{B}_\chi^T \boldsymbol{B} \boldsymbol{B}_L & \begin{pmatrix} \boldsymbol{B}_I^T \boldsymbol{A} \boldsymbol{B}_I + \boldsymbol{B}_\chi^T \boldsymbol{B} \boldsymbol{B}_I \\ + \boldsymbol{B}_I^T \boldsymbol{B} \boldsymbol{B}_\chi + \boldsymbol{B}_\chi^T \boldsymbol{D} \boldsymbol{B}_\chi \end{pmatrix} \end{bmatrix} dxdy \tag{4.4.14}$$

$$[K_{NL}] = \int \begin{bmatrix} 0 & B_L^T A B_{NL} \\ B_{NL}^T A B_L & \left(B_{NL}^T A B_I + B_I^T A B_{NL} + B_{NL}^T A B_{NL} + B_\chi^T B B_{NL} + B_{NL}^T B B_\chi \right) \end{bmatrix} dxdy \qquad (4.4.15)$$

$$[K_Q] = \int \begin{bmatrix} 0 & 0 \\ 0 & K_q \end{bmatrix} dxdy \qquad [K_q] = [S]^T \begin{bmatrix} N_x & N_{xy} \\ N_{xy} & N_y \end{bmatrix} [S] \qquad (4.4.16)$$

$$[K_{NL2}] = \int \begin{bmatrix} 0 & \frac{1}{2} B_L^T A B_{NL} \\ B_{NL}^T A B_L & \left(B_{NL}^T A B_I + \frac{1}{2} B_I^T A B_{NL} + \frac{1}{2} B_{NL}^T A B_{NL} + \frac{1}{2} B_\chi^T B B_{NL} + B_{NL}^T B B_\chi \right) \end{bmatrix} dxdy \qquad (4.4.17)$$

$$\{p\} = \int \begin{Bmatrix} B_L^T A b_e \\ \left(B_I^T A b_e + B_\chi^T B b_e + B_{NL}^T A b_e \right) \end{Bmatrix} dxdy \qquad (4.4.18)$$

$\{d^{(i)}\}$ is the displacement vector at the start of the i-th iteration and $\{\Delta d^{(i)}\}$ is the correction vector at the i-th iteration. $[K_T]$ is the symmetric tangent stiffness matrix evaluated at $\{d^{(i)}\}$. $[K_L]$ and $[K_{NL}]$ are the stiffness matrices with constant and variable coefficients respectively. $[K_Q]$ composes of direct and shearing stresses. The right hand side of equation (4.4.9) is the unbalanced force.

The matrices, defined in equations (4.4.4) to (4.4.7), compose of longitudinal trigonometric terms, polynomial functions for initial imperfection and polynomial crosswise shape functions. While constructing the stiffness matrices, integrations in the y direction, which only include the products of polynomial shape functions, are evaluated using Guassian quadrature. Integrations in the x direction, compose of the products of trigonometric terms or products of polynomial and trigonometric terms, are evaluated analytically. For those with products of polynomial and

trigonometric terms, reduction formula are applied to generate the exact values of the integrals. The formula are given in Chapter 3.3, equations (3.3.11) and (3.3.12).

The iterative process is repeated until the following convergence criterion is satisfied.

$$\frac{\left\|\Delta \boldsymbol{d}^{(i)}\right\|_2}{\left\|\boldsymbol{d}^{(i)}\right\|_2} \leq \tau \qquad (4.4.19)$$

where τ is the tolerance and $\|\boldsymbol{d}\|_2$ represents the l_2-norm of $\{\boldsymbol{d}\}$.

Once the vector $\{\boldsymbol{d}\}$ converges, displacements u, v and w at any point in any finite strip can be obtained by equations (4.2.1) and (4.2.6). Quantities of force and moment can also be determined by applying equations (4.1.4) - (4.1.7). The average longitudinal force acting on the whole plate corresponding to a prescribed end-shortening strain is defined as

$$N_{av} = \frac{1}{A} \sum \int_{-b/2}^{b/2} \int_0^A N_x(x, y) dx dy \qquad (4.4.20)$$

where the summation applies to all the finite strips.

4.5 VERIFICATION

The approach, introduced in the earlier part of this chapter, is tested by performing post-buckling analysis of an isotropic plate with symmetric initial imperfection. The length-to-thickness ratio A/h of the square plate is 120. The Poisson's ratio ν is 1/3. The loaded ends are of type A boundary and the unloaded edges are

free to wave laterally. All edges are simply supported in the out-of-plane direction. The initial imperfection, as shown in equation (4.5.1), is in the form of a single half sine wave in both the longitudinal and lateral directions.

$$w_o = w_{oh} \sin \frac{\pi x}{A} \sin \frac{\pi y}{A} \tag{4.5.1}$$

where w_{oh} is the amplitude of the initial imperfection.

A fourth order polynomial, as shown in equation (4.5.2), is used to simulate the longitudinal initial imperfection along each nodal line, by following the procedures described in Chapter 4.3. For the simply supported end condition, the constant term is assumed to be zero.

$$\sin \frac{\pi x}{A} \cong f_i(x) = 2.59 \cdot 10^{-2} x + 3.27 \cdot 10^{-5} x^2 - 4.14 \cdot 10^{-6} x^3 + 1.73 \cdot 10^{-8} x^4 \tag{4.5.2}$$

Post-buckling response is obtained by a finite strip model with eight quadratic strips over the whole plate. It is reasonable to assume that the deformed shape is of similar form to the initial imperfection, which is symmetric in both directions. Therefore, trigonometric series sin 2,4,6, cos 0,2,4,6 and sin 1,3 are selected to represent the displacement fields u, v and w in the longitudinal direction respectively.

Progressive end-shortening strains with 17 increments have been applied to the analysis. The number of iterations, which are required to satisfy the convergence criterion as specified in equation (4.4.19) with r = 0.0005, in each increment is shown in Table 4.3. Based on the Newton-Raphson procedure, not more than 13 iterations are required in all increments to achieve the accuracy in convergence. However, the rate of convergence is not uniform as

in the analysis of struts. Other numerical techniques, for example, the arc-length method, see Riks (1979) and Crisfield (1981), should be considered to adjust the increment automatically in order to improve the rate of convergence.

Table 4.3 Rate of convergence in each increment

increment	ε_o	No. of iter.
1	1.4878×10^{-4}	10
2	2.2204×10^{-4}	6
3	2.9529×10^{-4}	9
4	3.6855×10^{-4}	10
5	4.3180×10^{-4}	4
6	5.0506×10^{-4}	5
7	5.7631×10^{-4}	7
8	6.6157×10^{-4}	10
9	9.2796×10^{-4}	9
10	1.3044×10^{-3}	10
11	1.4508×10^{-3}	13
12	1.6451×10^{-3}	10
13	1.9035×10^{-3}	5
14	2.2550×10^{-3}	12
15	2.4063×10^{-3}	8
16	2.7027×10^{-3}	10
17	2.9791×10^{-3}	4

For $w_{oh} = 0.1h$, Figures 4.3 and 4.4 show the variations of load factor F with end-shortening strain ε_o and central deflection w_c (by the assumption that the maximum deflection is at the center of plate) respectively. The non-dimensional load factor is defined as $F = N_{av}A/\pi^2/E/h^3$.

Two other approaches have been reported to solve this problem. The first one was developed by Yamaki (1959), of which the post-buckling responses have been determined analytically. The second one, developed by Dawe, Wang and Lam (1995), used the finite strip method with initial imperfection represented by Fourier series. The graphical results by both approaches are also included in Figures

4.3 and 4.4. Close comparisons have been observed with the present approach.

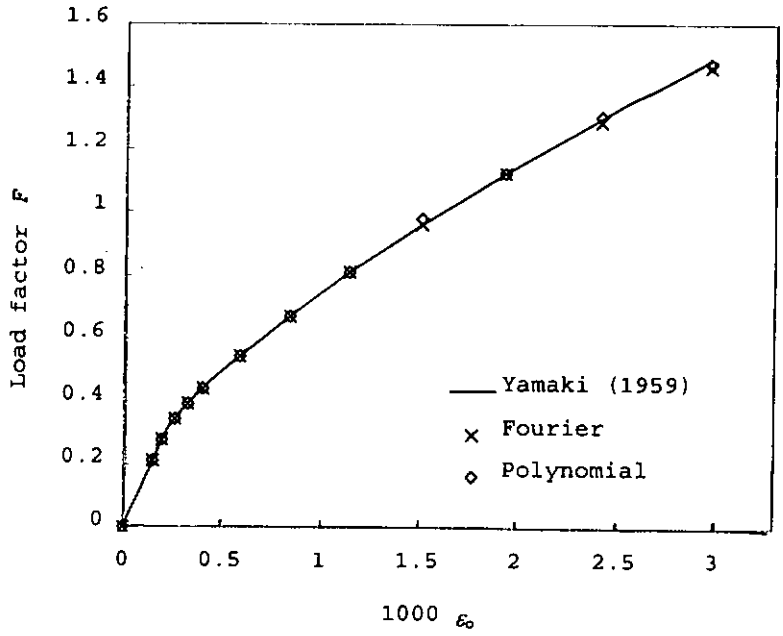

Figure 4.3 Isotropic plate with symmetric initial imperfection: variation of load factor with end-shortening strain

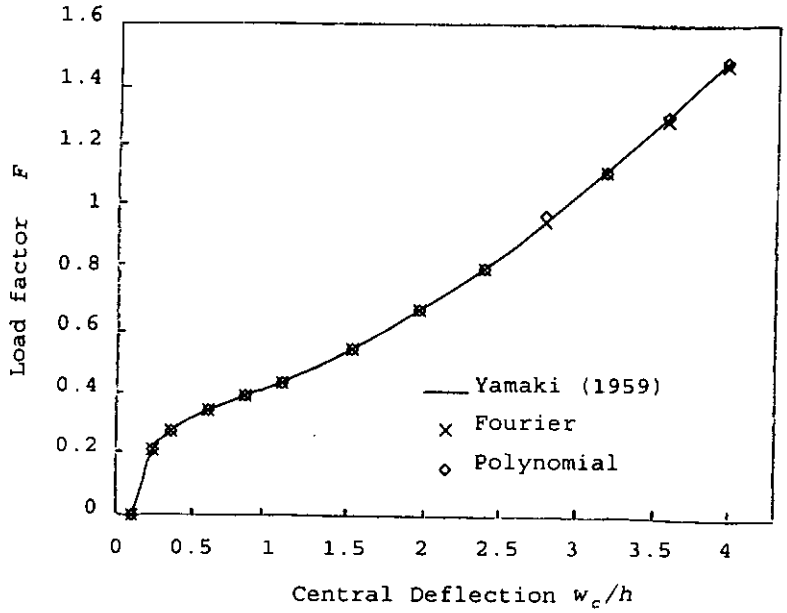

Figure 4.4 Isotropic plate with symmetric initial imperfection: variation of load factor with central deflection

Comparing with the analysis of struts in Chapter 3, demanding computational effort is involved in this analysis. The computations include integrations of the product of polynomial and trigonometric terms. In order to accurately represent the actual initial imperfection, high-order polynomial functions are used. However, it leads to increasing computational effort involving the exact integration by reduction formula, as shown in Chapter 4.4. Therefore, the present approach is not economical in cases when the imperfection can be simply expressed by trigonometric terms.

CHAPTER 5

PROGRAMMING TECHNIQUE FOR POST-BUCKLING ANALYSIS OF PLATES WITH GENERAL INITIAL IMPERFECTION

In this study, two computer codes written in standard FORTRAN 90 are developed and compiled by Lahey FORTRAN 90 v3.5 on a PC under Windows 98 environment. The two computer codes represent the development on the post-buckling analyses of struts and plates respectively. The basic structure of the computer procedures for the plate problem is best described by a flow chart as shown in Figure 5.1. Two specific procedures in the chart, due to the allowance of general initial imperfection, are discussed in this chapter.

In the procedure [INPUT DATA], information about material properties, coordinates, load increments, initial imperfection, coefficient of displacement fields, etc., are read and stored in the program. As defined in Chapter 4.2 and 4.3, displacements and initial imperfection along each longitudinal line are represented by Fourier series and polynomial functions, respectively. Fourier series for displacements u, v, and w are stored in two arrays of integers, NCOEF(50) and NFT(50). NCOEF(50) denotes the coefficients of Fourier series, and NFT(50), which is equal to 1 or -1, defines the cosine and sine terms. NFU, NFV and NFWB are the numbers of terms in $U_i(x)$, $V_i(x)$ and $W_i(x)$, respectively. For example, if the second term of the series for $V_i(x)$ is $\cos(3\pi x/A)$, integers 3 and 1 will be stored in NCOEF(NFU+2) and NFT(NFU+2), respectively. For the prescribed general initial imperfection, coefficients of polynomial along each nodal line are required. Integer NGIM and array WGVAL(500) are used for storing the degree and coefficients

of the polynomials, respectively. For example, the coefficient of x^m along the k-th nodal line is a, WGVAL((NGIM+1)*(k-1)+m+1) = a.

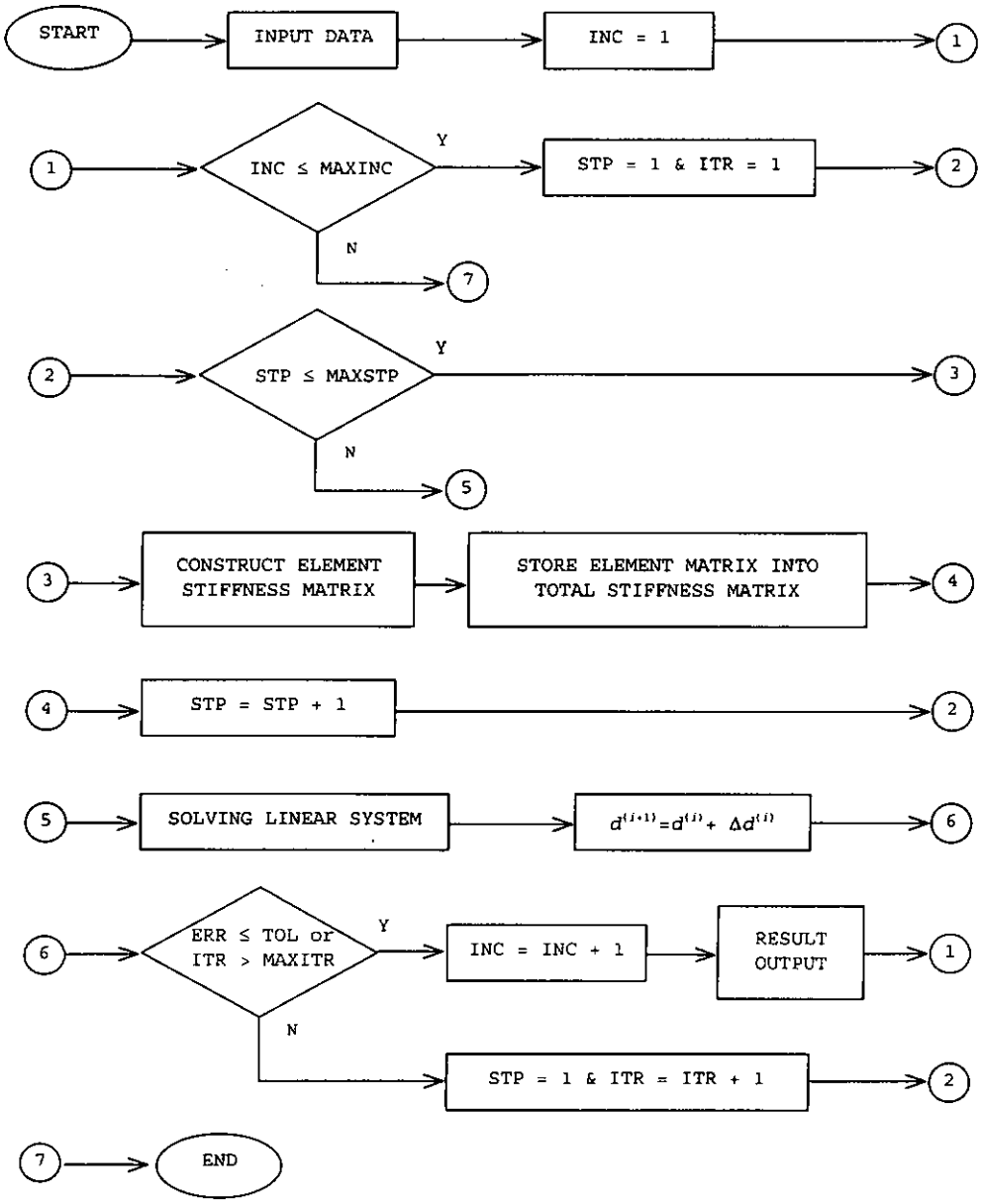

INC = load increment;

MAXINC = number of load increment;

STP = finite strip;

MAXSTP = number of finite strip;

ITR = iteration;

MAXITR = maximum number of iteration allowed;

$d^{(i)}$ = displacement vector at the start of the i-th iteration;

$\Delta d^{(i)}$ = correction vector in the i-th iteration;

ERR = $\left\|\Delta d^{(i)}\right\| / \left\|d^{(i)}\right\|$

TOL = tolerance

Figure 5.1 Program flow chart

[CONSTRUCT ELEMENT STIFFNESS MATRIX] is one of the most important procedures in the computer program. Matrices defined in equations (4.4.11) - (4.4.18) are constructed here. Table 5.1 shows the names of SUBROUTINEs for evaluating each entry in the matrices.

Table 5.1 SUBROUTINEs for the stiffness matrices

SUBROUTINE	Entry in stiffness matrices
LINEAR	$[B_L]^T[A][B_L]$, $[B_\chi]^T[D][B_\chi]$
LINR_I	$[B_L]^T[A][B_I]$, $[B_\chi]^T[B][B_I]$, $[B_I]^T[A][B_I]$
LINR_B	$[B_L]^T[B][B_\chi]$
NONLK1	$[B_{NL}]^T[A][B_L]$, $[A]\{\varepsilon_{NL}\}$
NLK1_I	$[B_{NL}]^T[A][B_I]$
NLK1_B	$[B_{NL}]^T[B][B_\chi]$
NONLK2_WANDV	$[B_{NL}]^T[A][B_{NL}]$
GEOMEK	$\varepsilon_o[A]\{b_e\}$
GEOMUV	$[A]\{\varepsilon_L\}$
GEOMI	$[A]\{\varepsilon_I\}$
GEOMB	$[B]\{\chi\}$
VECTA	$[B_L]^T[A]\{b_e\}$
VECTI	$[B_I]^T[A]\{b_e\}$
VECTB	$[B_\chi]^T[B]\{b_e\}$

where

$$\{N\} = \begin{Bmatrix} N_x \\ N_y \\ N_{xy} \end{Bmatrix} = \varepsilon_o[A]\{b_e\} + [A]\{\varepsilon_L\} + [A]\{\varepsilon_I\} + [A]\{\varepsilon_{NL}\} + [B]\{\chi\} \qquad (5.1.1)$$

For the SUBROUTINEs involving matrix $[B_I]$, the polynomial terms due to the initial imperfection are included. Integrations of the product of polynomial and trigonometric functions are required. SUBROUTINEs, XNT1, XNT2 and XNT3 are developed for integrating the

products of a polynomial term with one, two and three trigonometric terms respectively. Equations (5.1.2) - (5.1.7) show the mathematical formula used in the SUBROUTINEs, XNT1, XNT2 and XNT3. Figures 5.2 and 5.3 show the flow charts of SUBROUTINEs XNT2 and XNT1. Other SUBROUTINE XNT3 can be evaluated in similar manner.

$$S_m C_n = \frac{1}{2}(S_{m+n} + S_{m-n}) \qquad (5.1.2)$$

$$C_m S_n = \frac{1}{2}(S_{m+n} - S_{m-n}) \qquad (5.1.3)$$

$$C_m C_n = \frac{1}{2}(C_{m+n} + C_{m-n}) \qquad (5.1.4)$$

$$S_m S_n = \frac{1}{2}(C_{m-n} - C_{m+n}) \qquad (5.1.5)$$

$$I_k^{(s)} = -\frac{L^k}{m}\cos mL + \frac{k}{m} I_{k-1}^{(c)} \qquad (5.1.6)$$

$$I_k^{(c)} = \frac{L^k}{m}\sin mL - \frac{k}{m} I_{k-1}^{(s)} \qquad (5.1.7)$$

where $I_k^{(s)} = \int_0^L x^k \sin mx\, dx$, $I_k^{(c)} = \int_0^L x^k \cos mx\, dx$, $S_m = \sin\frac{m\pi x}{L}$ and $C_m = \cos\frac{m\pi x}{L}$.

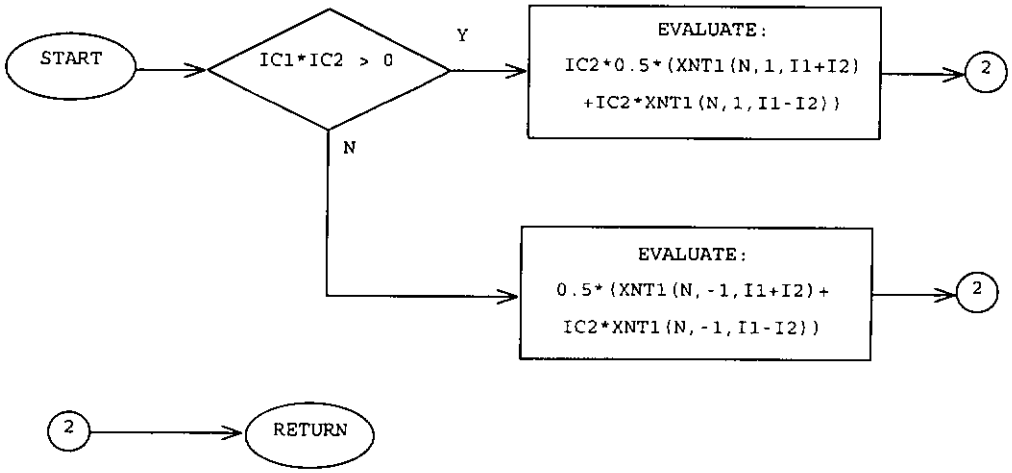

Figure 5.2 SUBROUTINE XNT2(N,IC1,IC2,I1,I2)

where N is the order of a polynomial term. In order to consider all the terms in the polynomial, it is easy to use a DO loop to generate them. IC1, IC2, I1 and I2 describe the trigonometric terms due to the displacements. IC1 and IC2, stored in NFT(50) and are equal to 1 or -1, are used to define the cosine or sine term. I1 and I2 are the coefficients of trigonometric terms. By using these representations, the mathematical formula can be programmed easily.

In the chart of XNT2, see Figure 5.2, the integration with two trigonometric terms is separated into two integrals with single trigonometric term. SUBROUTINE XNT1 is used to integrate the product of one polynomial and one trigonometric term.

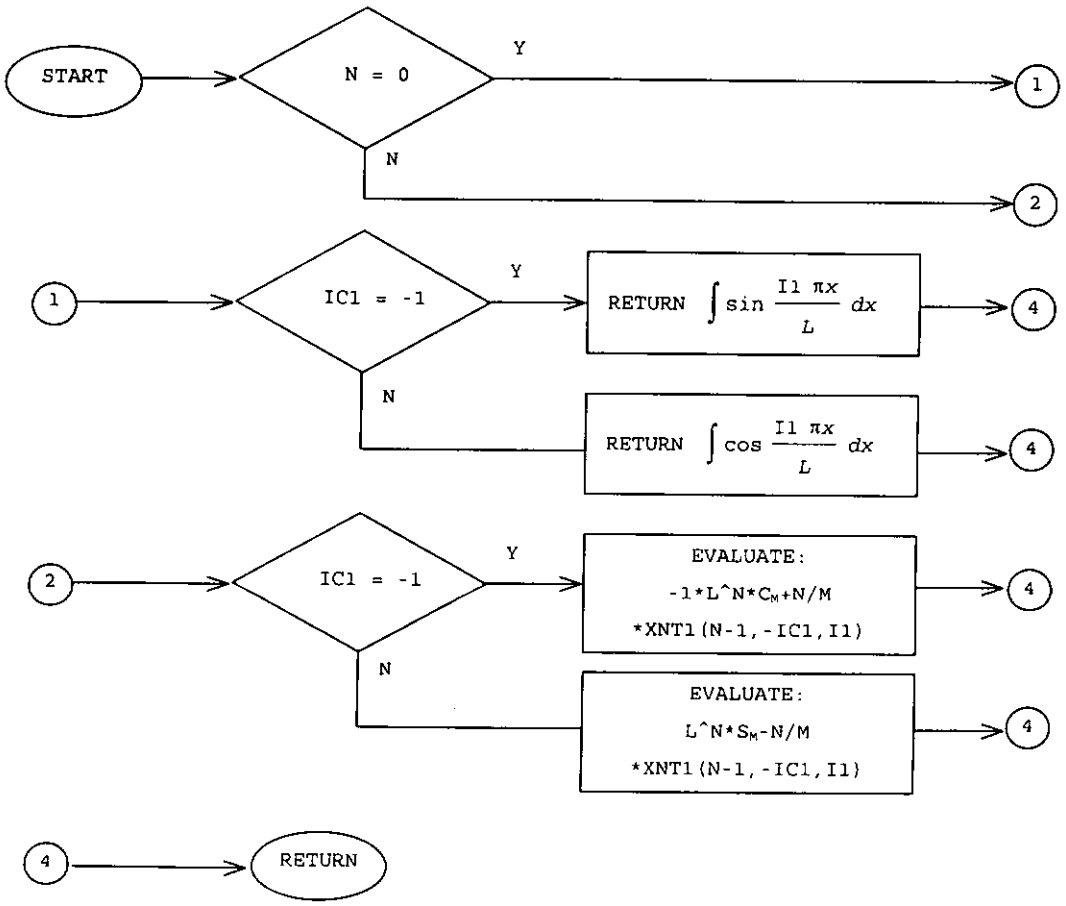

Figure 5.3 SUBROUTINE XNT1(N,IC1,I1)

Figure 5.3 shows that exact integration can be generated by recursive iteration. The program, which follows the procedures above, can be developed easily.

Other numerical techniques, for example, Guassian quadrature, see Atkinson (1989), for the integration of polynomials in the y direction, are implemented in the usual manner and will not be discussed in this chapter.

CHAPTER 6

CASE STUDIES OF PLATES WITH INITIAL IMPERFECTIONS

Using the finite strips developed in Chapter 5, several applications are presented in this chapter. Non-symmetric imperfections, which may not be easily solved by previous approaches, are also included. In the first application, initial imperfections of the isotropic plates are in various forms of polynomial functions. Using the unsymmetric cross-ply and anisotropic laminates as examples, initial imperfections in the form of trigonometric functions are considered. An arbitrary initial imperfection, without exact functional form, is considered in the third application. Different in-plane boundary conditions along both the loaded and unloaded edges are also prescribed in each application.

6.1 ISOTROPIC PLATES WITH POLYNOMIAL INITIAL IMPERFECTIONS

The square isotropic plate considered here is with unit thickness and length A = 120. The Poisson's ratio ν is 1/3. The loaded ends are of Type A boundary and the unloaded edges are free to wave. All edges are simply supported in the out-of-plane direction.

6.1.1 Symmetric Initial Imperfections with Constant Curvature

The initial imperfection is in the form of constant curvature in the x direction and in the form of a half sine wave in the y

direction. Recalling the definition of w_o in Chapter 4.3, the longitudinal expression $f_i(x)$ satisfies the condition

$$\frac{d^2 f_i(x)}{dx^2} = \text{constant} \qquad (6.1.1)$$

A quadratic polynomial is used to represent this imperfection. Maximum initial imperfection is assumed to be at the mid-point of each nodal line and the magnitude is w_{oh}. Therefore,

$$\left.\frac{df_i(x)}{dx}\right|_{x=\frac{A}{2}} = 0; \quad f_i\left(\frac{A}{2}\right) = 1 \qquad (6.1.2)$$

Combine with the out-of-plate conditions at the strip ends,

$$f_i(x) = 3.33 \cdot 10^{-2} x - 2.78 \cdot 10^{-4} x^2 \qquad (6.1.3)$$

The response of the plate when subjected to progressive uniform end-shortening is obtained by using eight quadratic strips over the whole plate. For the trigonometric series representation, it is reasonable to use only even terms for u and v and odd terms for w, see Dawe, Lam and Azizian (1992) and Dawe, Wang and Lam (1995). It is by the assumption that the deformations of isotropic plates are symmetric, which are similar to the shape of imperfection. However, both odd and even terms, sin 1-6, cos 0-6 and sin 1-5 for displacements u, v and w respectively, are included in this study. This representation enables non-symmetric deformations to be considered in latter analyses, which are with non-symmetric initial imperfections.

It is obvious that the deformation is in the form of a single half sine wave and the maximum deflection is at the centre.

Graphical results are presented in Figures 6.1 and 6.2 of load factor $F = N_{av}A/\pi^2/E/h^3$ versus end-shortening strain ε_o, and versus central deflection w_c, respectively. Two values of w_{oh} (w_{oh} = 0.2 and w_{oh} = 2.0) are considered. Note that the effect of initial imperfection increases with the magnitude of imperfection.

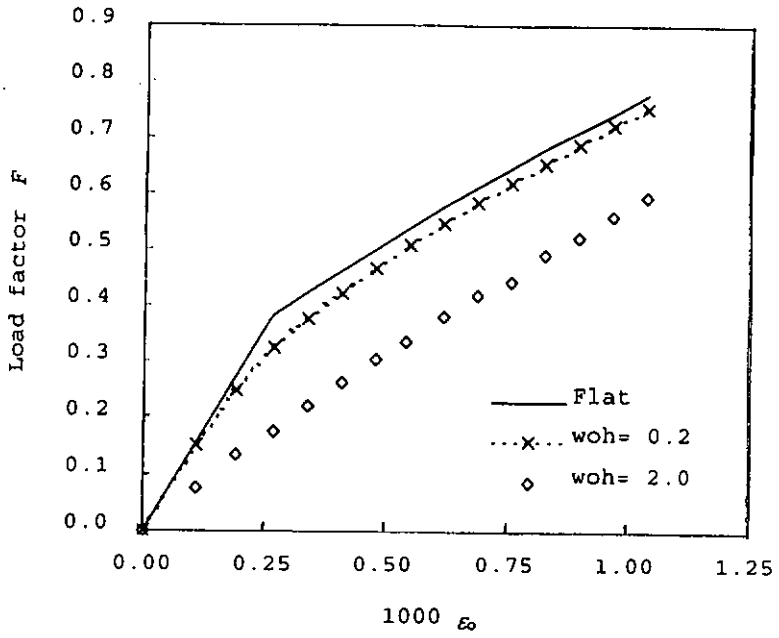

Figure 6.1 Isotropic plates with constant curvature: variation of load factor with end-shortening strain

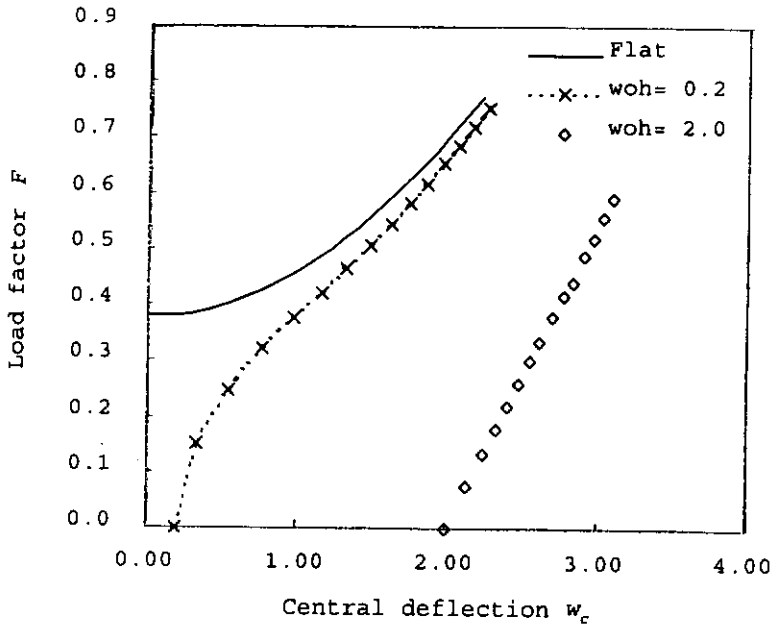

Figure 6.2 Isotropic plates with constant curvature: variation of load factor with central deflection

6.1.2 Non-symmetric Initial Imperfections

With the same material properties and boundary conditions, two problems with different non-symmetric initial imperfections are considered. The initial imperfections are in the form of cubic polynomials in the x direction and a half sine wave in the y direction. The maximum initial imperfections are at $x = x'$, which may not necessary be at the mid-point.

$$\left.\frac{df_i(x)}{dx}\right|_{x=x'} = 0 ; \quad f_i(x') = 1 \qquad (6.1.4)$$

Consistent with the above conditions, $f_i(x)$ can be expressed by equations (6.1.5) and (6.1.6) for $x' = 45$ and $x' = 30$ respectively.

$$f_i(x) = 4.98 \cdot 10^{-2}x - 7.31 \cdot 10^{-4}x^2 + 2.63 \cdot 10^{-6}x^3 \qquad (6.1.5)$$

$$f_i(x) = 7.41 \cdot 10^{-2}x - 1.60 \cdot 10^{-3}x^2 + 8.23 \cdot 10^{-6}x^3 \qquad (6.1.6)$$

The post-buckling responses of plates, with w_{oh} = 0.2 and w_{oh} = 2.0, are obtained by using the previous finite strip model. Variations of load factor with end-shortening strain for both magnitudes of imperfections are shown in Figures 6.3 and 6.4.

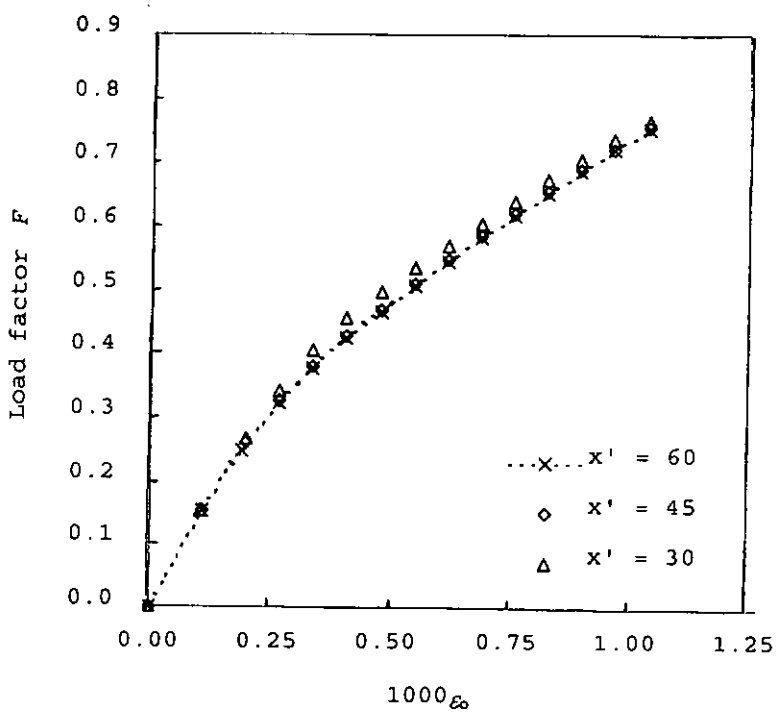

Figure 6.3 Isotropic plates with cubic initial imperfections (w_{oh} = 0.2): variation of load factor with end-shortening strain

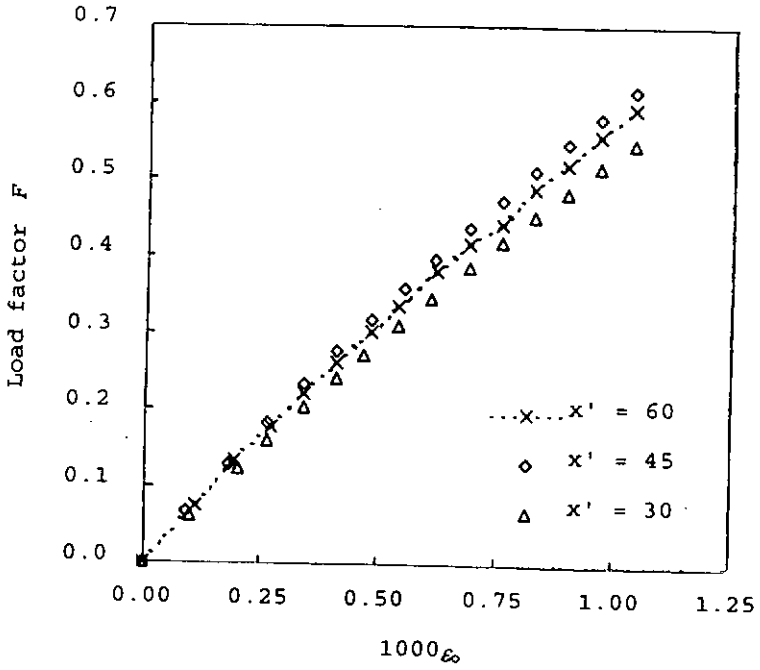

Figure 6.4 Isotropic plates with cubic initial imperfections (w_{oh} = 2.0): variation of load factor with end-shortening strain

The total deflection, $w_t = w + w_o$, along the nodal line at the centre is used to represent the deformed shape of the whole plate, as the initial imperfections are symmetric in the y direction. Variations of w_t for both cases are shown in Figures 6.5 and 6.6.

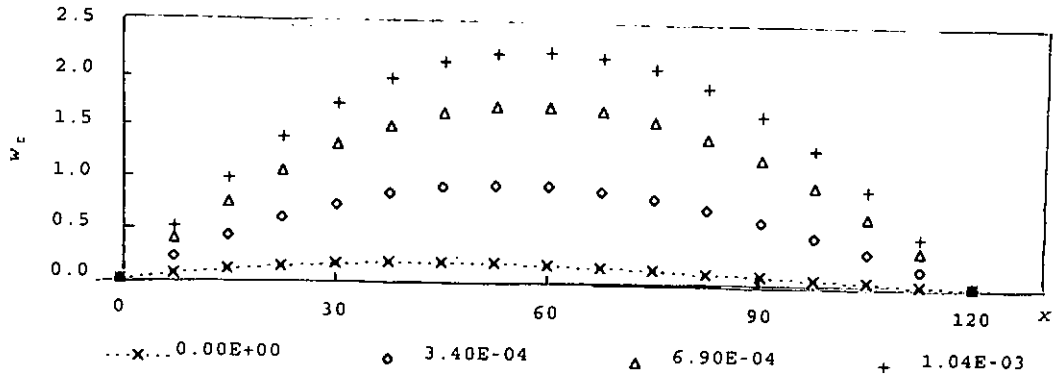

(a)

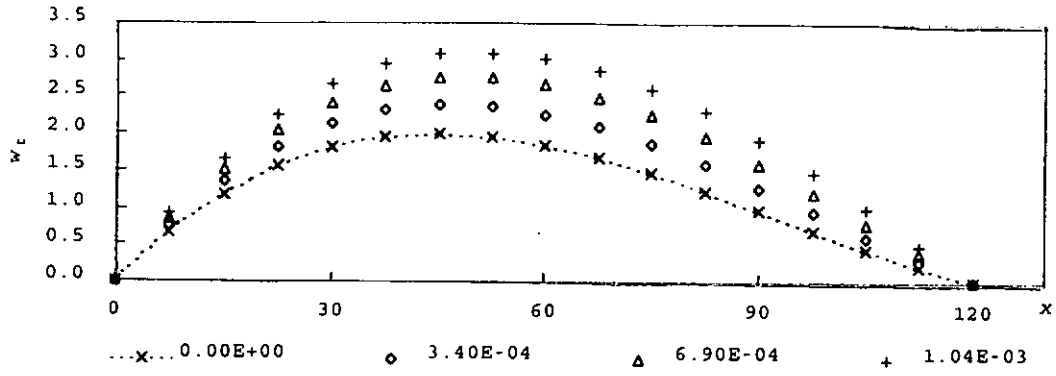

(b)

Figure 6.5 Isotropic plates with cubic initial imperfections (x' = 45): variations of w_t at four levels of end-shortening strain; w_{oh} = 0.2 and (b) w_{oh} = 2.0

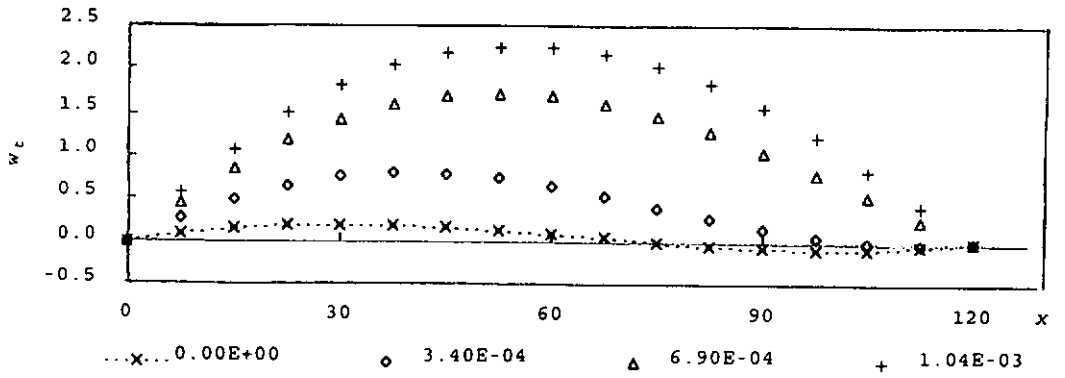

(a)

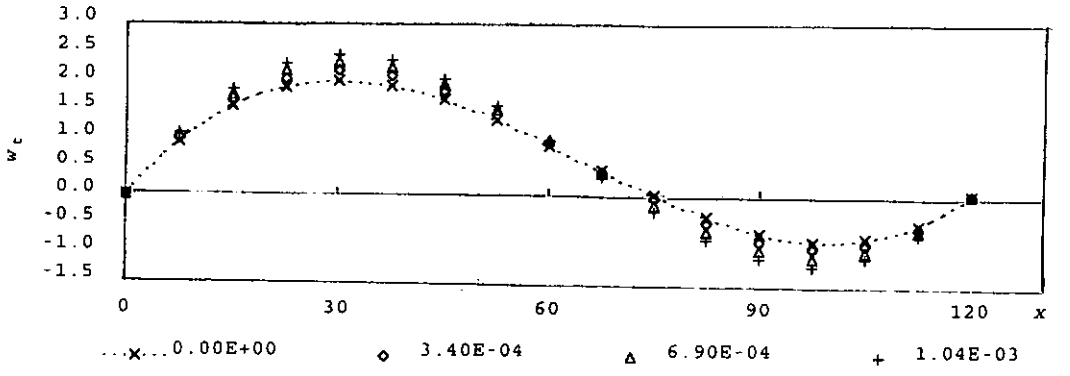

(b)

Figure 6.6 Isotropic plates with cubic initial imperfections (x' = 30): variations of w_t at four levels of end-shortening strain; (a) w_{oh} = 0.2 and (b) w_{oh} = 2.0

Firstly, maximum deflections w_t do not occur at the mid-point while the initial imperfections are non-symmetric in the x direction. Tables 6.1 and 6.2 show the maximum w_t with their locations along the central nodal line for both magnitudes of initial imperfection. In the case of x' = 45, the deformations tend to be in a single half sine wave for both magnitudes. When x' = 30, responses for both w_{oh} are different. The deformed shape, for w_{oh} = 0.2, tends to behave in a half sine wave and is similar to those for x' = 60 and x' = 45 at high strain level. This is shown in Figure 6.6(a) and Table 6.1. However, the plate with w_{oh} = 2.0 deforms to two half sine waves, as shown in Figure 6.6(b), whilst only a single half sine wave can be observed for the other two cases. It demonstrates that the magnitude of initial imperfection not only affects the magnitude of deformation but also the deformed shape for non-symmetric initial imperfection.

Table 6.1 Comparison of maximum total deflection for different x' with w_{oh} = 0.2; [Values in parenthesis denote the location of the maximum defection]

ε_o	Flat plate	x'=60	x'=45	x'=30
0.00E+00	-	0.20 (x =60.00)	0.20 (x =45.00)	0.20 (x =30.00)
3.40E-04	0.75 (x =60.00)	0.98 (x =60.00)	0.96 (x =54.40)	0.58 (x =36.41)
6.90E-04	1.69 (x =60.00)	1.75 (x =60.00)	1.74 (x =57.62)	1.72 (x =52.04)
1.04E-03	2.24 (x =60.00)	2.27 (x =60.00)	2.27 (x =58.59)	2.25 (x =55.48)

Table 6.2 Comparison of maximum total deflection for different x' with w_{oh} = 2.0; [Values in parenthesis denote the location of the maximum defection]

ε_o	Flat plate	x'=60	x'=45	x'=30
0.00E+00	-	2.00 (x =60.00)	2.00 (x =45.00)	2.00 (x =30.00)
3.40E-04	0.75 (x =60.00)	2.41 (x =60.00)	2.40 (x =46.83)	2.17 (x =30.42)
6.90E-04	1.69 (x =60.00)	2.78 (x =60.00)	2.77 (x =48.49)	2.32 (x =30.66)
1.04E-03	2.24 (x =60.00)	3.11 (x =60.00)	3.10 (x =49.86)	2.45 (x =30.77)

6.2 UNSYMMETRIC CROSS-PLY LAMINATES WITH TRIGONOMETRIC INITIAL IMPERFECTIONS

In the above examples, the coefficient matrix [$\boldsymbol{B}$] vanishes due to isotropic behavior. In this application, cross-plies having unsymmetric layup arrangement, i.e. with non-zero matrix [$\boldsymbol{B}$], are considered. Discussion on the coefficient matrices has been presented in Chapter 4.1. The rectangular laminates are of length A = 120, width B = 60 and with unit thickness. They are made up of four layers of equal thickness lamina in a $[0/90]_2$ assembly. Layer properties are E_L = 400, E_T = 10, G_{LT} = 5 and ν_{LT} = 0.25. The coefficient matrices [$\boldsymbol{A}$], [$\boldsymbol{B}$] and [$\boldsymbol{D}$], as shown in equations (6.2.1)-(6.2.3), are consistent with the properties in Table 4.1.

$$[\boldsymbol{A}] = \begin{bmatrix} 205.0 & 2.5 & 0.0 \\ 2.5 & 205.0 & 0.0 \\ 0.0 & 0.0 & 5.0 \end{bmatrix} \tag{6.2.1}$$

$$[\boldsymbol{B}] = \begin{bmatrix} -24.4 & 0.0 & 0.0 \\ 0.0 & 24.4 & 0.0 \\ 0.0 & 0.0 & 0.0 \end{bmatrix} \tag{6.2.2}$$

$$[D] = \begin{bmatrix} 17.1 & 0.2 & 0.0 \\ 0.2 & 17.1 & 0.0 \\ 0.0 & 0.0 & 0.4 \end{bmatrix} \qquad (6.2.3)$$

Edges of the laminated plate are out-of-plane simply supported. The analysis is of Type A boundary along the loaded edges and the unloaded edges are free to wave. Two initial imperfections in the form of trigonometric functions, with maximum magnitude $w_{oh} = 0.35$ located at the centre, are considered.

6.2.1 Symmetric Initial Imperfection

The first initial imperfection, defined in equation (6.2.4), is symmetric and in form of a half sine wave in both x and y directions.

$$w_o = w_{oh} \sin\frac{\pi x}{120} \sin\frac{\pi y}{60} \qquad (6.2.4)$$

In order to approximate the non-symmetric initial imperfection in the second case accurately, sixth order polynomial functions are used to simulate the longitudinal imperfection, whilst only a forth order polynomial functions have been used for symmetric imperfection in the application of Chapter 4.5.

$$\sin\frac{\pi x}{120} \cong f_i(x) = 2.62 \cdot 10^{-2}x - 1.24 \cdot 10^{-6}x^2 - 2.91 \cdot 10^{-6}x^3 - 2.65 \cdot 10^{-9}x^4 + 1.48 \cdot 10^{-10}x^5 - 4.10 \cdot 10^{-13}x^6 \qquad (6.2.5)$$

The whole laminate is analyzed with sin 1-6, cos 0-6 and sin 1-5 series being the representation for u, v and w respectively. Figure 6.7 shows the variation of load factor with end-shortening

strain. Two equilibrium paths can be traced. The first one shows that the laminate deforms initially to a single half sine wave and then changes to two half sine waves. The other equilibrium path shows a change from one to three half sine waves. Since the first equilibrium path is at lower strain level, the change from one to two waves occurs first. The deformed shape with three half sine waves may be observed at a higher level of strain when the two equilibrium paths match. Deformed shapes of the laminate, following both equilibrium paths, are shown in Figures 6.8 and 6.9. Discussions on the change in deformed shapes were presented in previous studies, Onate and Suarez (1983), Shin, Griffin and Gurdal (1993) and Shiau and Wu (1995). Dawe, Wang and Lam (1995) have also developed an approach, of which the initial imperfection is represented by the same Fourier series. Comparisons of results from both approaches are also included in Figure 6.7. Very similar results are obtained.

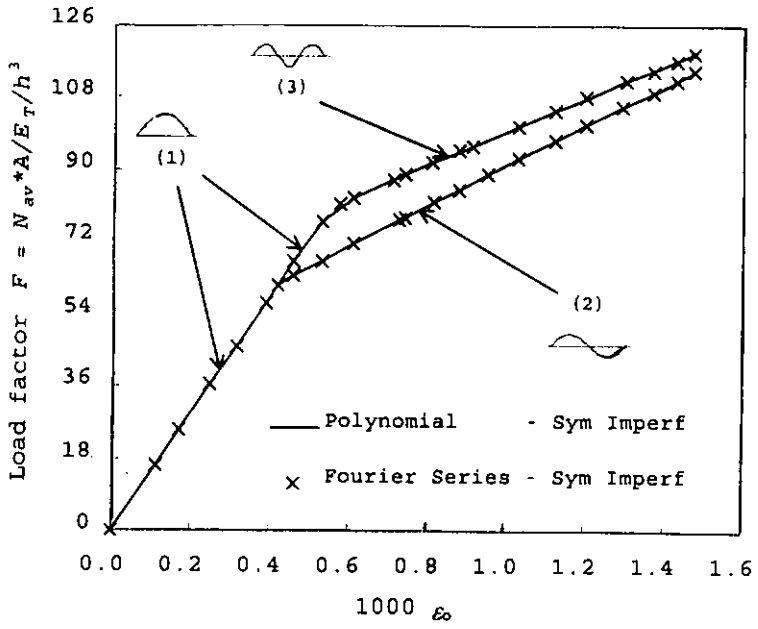

Figure 6.7 Unsymmetric cross-ply laminate with symmetric initial imperfection: variation of load factor with end-shortening strain; [Values in parentheses, (2) etc., denotes the number of longitudinal half waves]

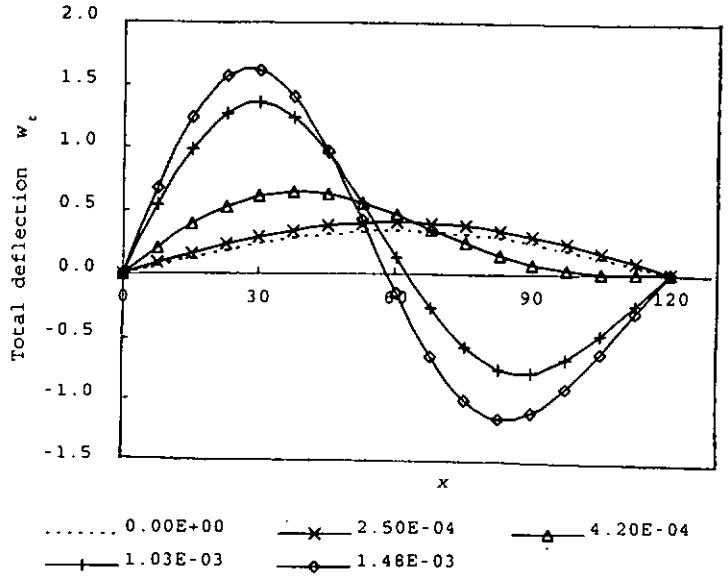

Figure 6.8 Unsymmetric cross-ply laminate with symmetric initial imperfection: variations of w_t along the longitudinal central line at five levels of end-shortening strain; with the equilibrium path for two half sine waves

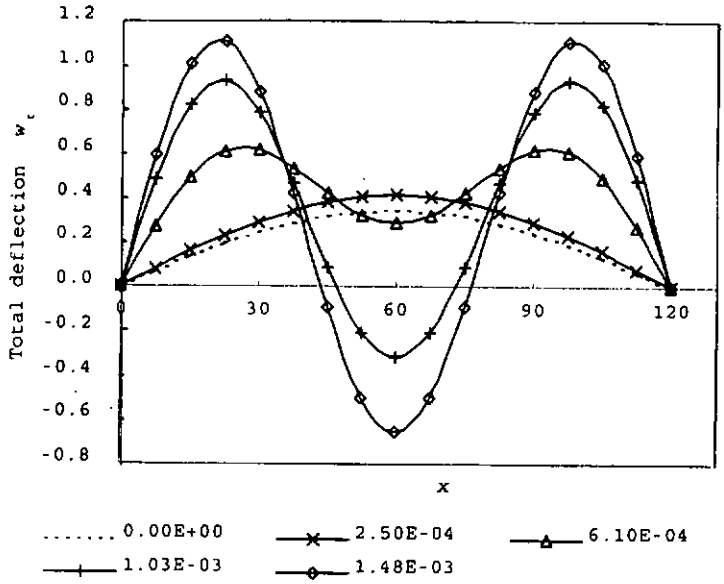

Figure 6.9 Unsymmetric cross-ply laminate with symmetric initial imperfection: variations of w_t along the longitudinal central line at five levels of end-shortening strain; with the equilibrium path for three half sine waves

6.2.2 Non-symmetric Initial Imperfection

The second initial imperfection is symmetric in the y direction, and is non-symmetric in the x direction. The initial imperfection is expressed as

$$w_o = w_{oh} \cdot F(x) \cdot \sin \frac{\pi y}{60} \tag{6.2.6}$$

where

$$F(x) = \begin{cases} \sin \dfrac{\pi x}{120} & \text{for } 0 \le x < 60 \\ \dfrac{1}{2}\left[1 + \cos \dfrac{2\pi(x - 60)}{120}\right] & \text{for } 60 \le x \le 120 \end{cases} \tag{6.2.7}$$

The first interval ($0 \le x < 60$) is half of a half sine wave. The

second interval is represented by a different trigonometric function such that the curvature changes to negative sign between the range $60 \leq x \leq 120$. Figure 6.10 shows the difference between the forms of both symmetric and non-symmetric initial imperfections.

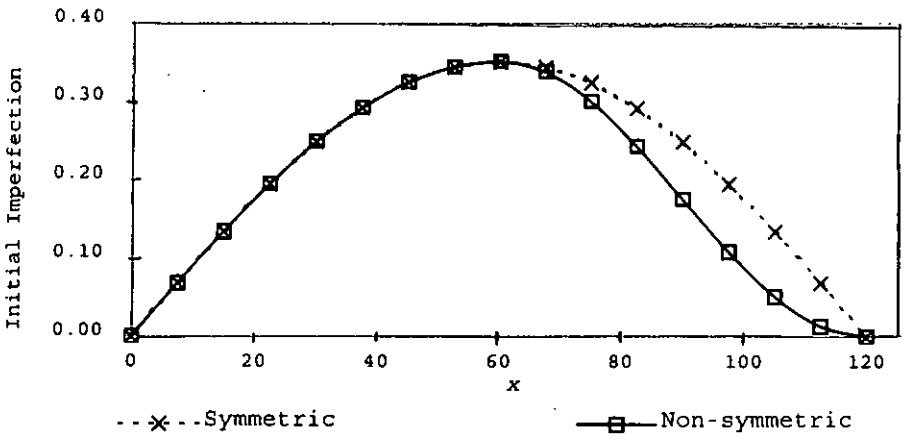

Figure 6.10 Symmetric, equation (6.2.4), and non-symmetric, equation (6.2.7), trigonometric initial imperfections

Using the previous approach by Dawe, Wang and Lam (1995), the initial imperfection will have to be represented by Fourier series. Complicated series will be needed to simulate the two intervals separately in the x direction.

In this case, the longitudinal shape of initial imperfection is represented by a single sixth order polynomial function.

$$F_i(x) \equiv f_i(x) = 3.26 \cdot 10^{-2}x - 7.66 \cdot 10^{-4}x^2 + 2.64 \cdot 10^{-5}x^3 - 4.73 \cdot 10^{-7}x^4 + 3.36 \cdot 10^{-9}x^5 - 8.03 \cdot 10^{-12}x^6 \quad (6.2.8)$$

Based on the finite strip model in Chapter 6.2.1, the load factor against end-shortening strain curve for this imperfection is included in Figure 6.11. Figure 6.12 shows the total deflection w_t along the central nodal line of the laminate at five different

levels of end-shortening strains. Due to the change in signs of the curvature, the laminate deforms initially to two half sine waves when the in-plane loading is applied. Compared with the case with symmetric imperfection, out-of-plane deformation of the laminate is firstly in the form of a single half sine wave, and then changes to two half sine waves on increasing end-shortening strain.

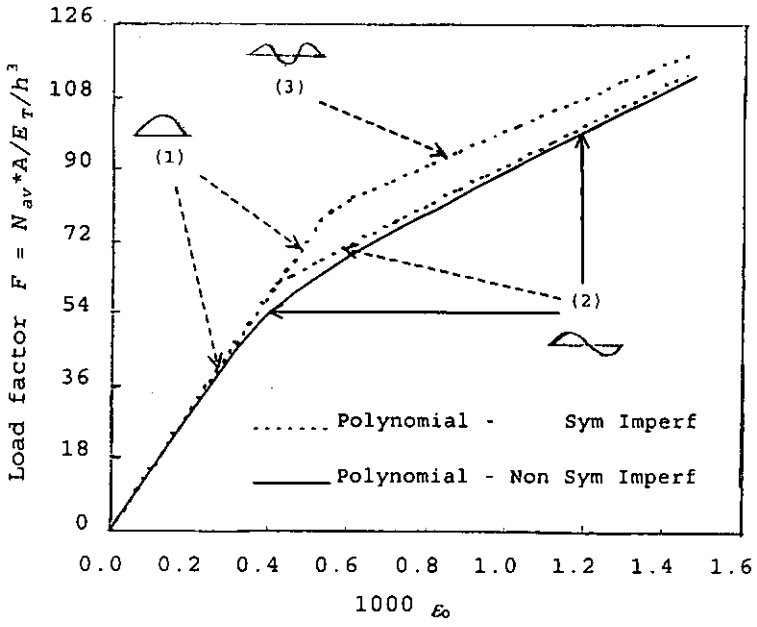

Figure 6.11 Unsymmetric cross-ply laminates with non-symmetric initial imperfections: variation of load factor with end-shortening strain; [Values in parentheses, (2) etc., denotes the number of longitudinal half waves]

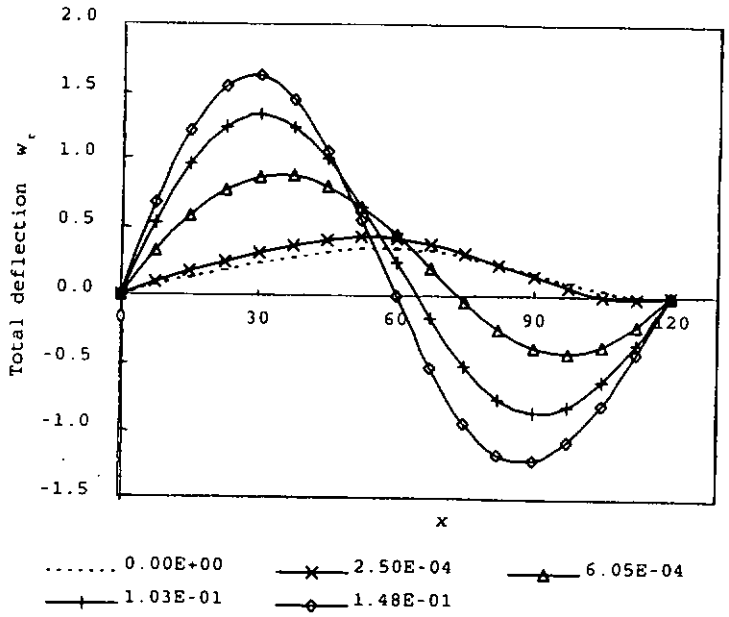

Figure 6.12 Unsymmetric cross-ply laminate with non-symmetric initial imperfection: variation of w_t along longitudinal central line at five levels of end-shortening strain

6.3 UNSYMMETRIC CROSS-PLY LAMINATES WITH ARBITRARY INITIAL IMPERFECTIONS

The problem considered here is of Type B, which the loaded ends are held against any lateral expansion. The lateral movement along the unloaded edges is also restrained completely, i.e. all the lateral displacement coefficients v_{im} along those edges are set to be zero. For out-of-plane behavior, all edges are simply supported. The laminate is made up of four layers $[0/90]_2$ and with the layer properties: E_L = 400, E_T = 10, G_{LT} = 5 and ν_{LT} = 0.25. The square laminate is of length A = 100 and unit thickness. That is, material properties are the same as those in Chapter 6.2, but the sizes are different.

The contour plot in Figure 6.13 shows an arbitrary initial imperfection, with exact functional form not known.

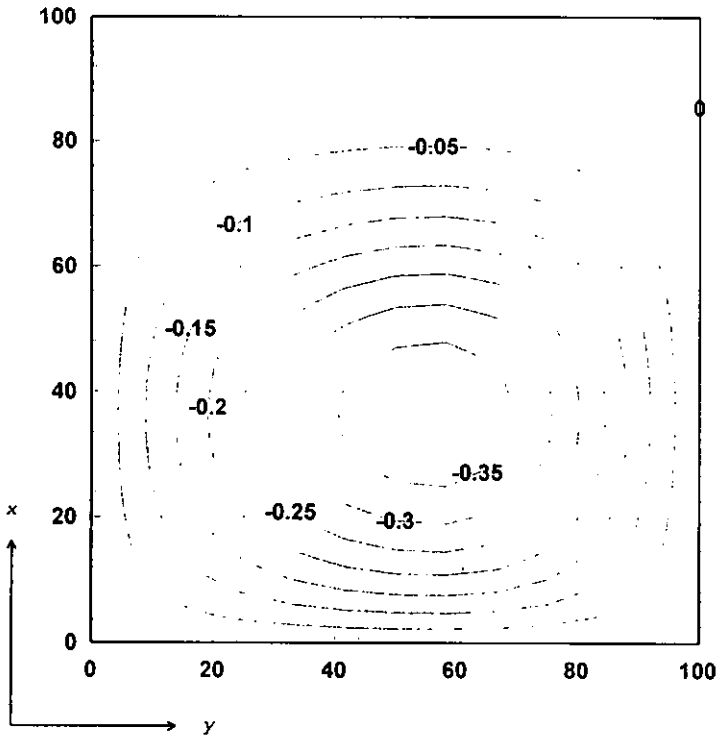

Figure 6.13 Contour plot of the initial imperfection w_o

Along each nodal line, ten discrete magnitudes of initial imperfection are obtained. Applying the least-squares technique introduced in Chapter 3.2.2, sixth order polynomial functions are used to describe the imperfection. Coefficients of each polynomial are shown in Table 6.3. Two other cases, either the laminate is flat or the magnitude of its initial imperfection is enlarged by a factor of 20/3, are also considered for comparison.

Table 6.3 Coefficients of polynomial function for initial imperfection along each nodal line; [coefficients along both unloaded edge and all constant terms are zero]

		Coefficients					
i	y	x	x^2	x^3	x^4	x^5	x^6
1	0.00	0.00E+00	0.00E+00	0.00E+00	0.00E+00	0.00E+00	0.00E+00
2	4.17	-2.91E-03	7.64E-05	-2.08E-06	4.90E-08	-5.19E-10	1.90E-12
3	8.33	-5.72E-03	1.50E-04	-4.09E-06	9.63E-08	-1.02E-09	3.73E-12
4	12.50	-8.38E-03	2.20E-04	-6.00E-06	1.41E-07	-1.49E-09	5.47E-12
5	16.67	-1.09E-02	2.85E-04	-7.77E-06	1.83E-07	-1.94E-09	7.10E-12
6	20.83	-1.32E-02	3.46E-04	-9.42E-06	2.22E-07	-2.35E-09	8.60E-12
7	25.00	-1.53E-02	4.01E-04	-1.09E-05	2.57E-07	-2.73E-09	9.98E-12
8	29.17	-1.72E-02	4.52E-04	-1.23E-05	2.90E-07	-3.07E-09	1.12E-11
9	33.33	-1.89E-02	4.97E-04	-1.35E-05	3.19E-07	-3.38E-09	1.24E-11
10	37.50	-2.04E-02	5.37E-04	-1.46E-05	3.44E-07	-3.65E-09	1.33E-11
11	41.67	-2.17E-02	5.71E-04	-1.55E-05	3.66E-07	-3.87E-09	1.42E-11
12	45.83	-2.27E-02	5.98E-04	-1.63E-05	3.83E-07	-4.06E-09	1.49E-11
13	50.00	-2.35E-02	6.17E-04	-1.68E-05	3.95E-07	-4.19E-09	1.53E-11
14	54.17	-2.38E-02	6.26E-04	-1.71E-05	4.01E-07	-4.25E-09	1.56E-11
15	58.33	-2.38E-02	6.26E-04	-1.70E-05	4.01E-07	-4.25E-09	1.56E-11
16	62.50	-2.33E-02	6.13E-04	-1.67E-05	3.93E-07	-4.16E-09	1.52E-11
17	66.67	-2.23E-02	5.87E-04	-1.60E-05	3.76E-07	-3.99E-09	1.46E-11
18	70.83	-2.08E-02	5.48E-04	-1.49E-05	3.51E-07	-3.72E-09	1.36E-11
19	75.00	-1.88E-02	4.94E-04	-1.34E-05	3.16E-07	-3.35E-09	1.23E-11
20	79.17	-1.62E-02	4.26E-04	-1.16E-05	2.73E-07	-2.89E-09	1.06E-11
21	83.33	-1.32E-02	3.47E-04	-9.45E-06	2.22E-07	-2.36E-09	8.62E-12
22	87.50	-9.83E-03	2.58E-04	-7.04E-06	1.66E-07	-1.76E-09	6.42E-12
23	91.67	-6.32E-03	1.66E-04	-4.53E-06	1.06E-07	-1.13E-09	4.13E-12
24	95.83	-2.81E-03	7.37E-05	-2.01E-06	4.73E-08	-5.01E-10	1.83E-12
25	100.00	0.00E+00	0.00E+00	0.00E+00	0.00E+00	0.00E+00	0.00E+00

Responses of the laminates are predicted by twelve quadratic finite strips, with the longitudinal series representation sin 1-6, sin 1-6 and sin 1-5 for u, v and w respectively. Variations of load factor with end-shortening strain are shown in Figure 6.14. Similar responses between the flat laminate and the laminate with small arbitrary imperfection can be observed. Less force is required in the analysis with the enlarged imperfection, as compared with the other two cases.

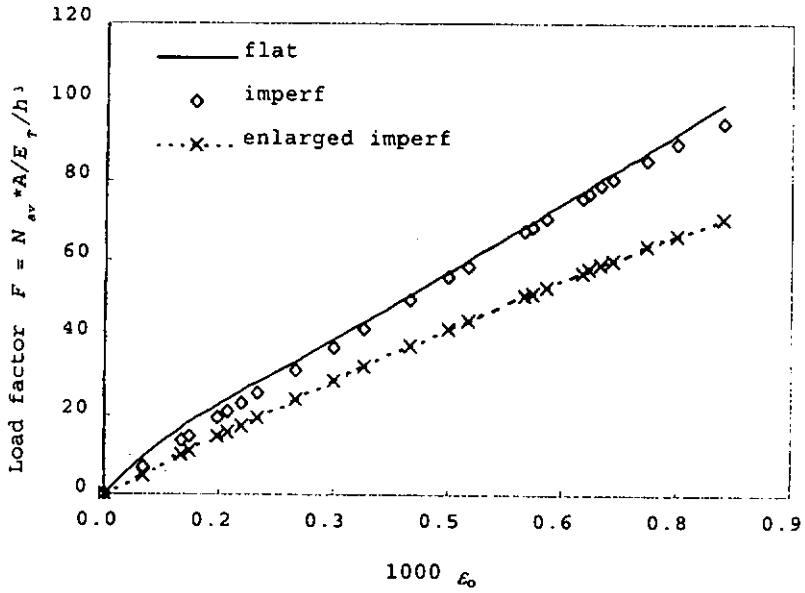

Figure 6.14 Unsymmetric cross-ply laminates with arbitrary initial imperfections: variations of load factor with end-shortening strain

Figure 6.15 shows the total deformation w_t of a flat laminate along the nodal line y = 25, 50 and 75, which is in the form of a half sine wave. Because of the presence of non-zero matrix $[B]$, out-of-plane deformations are initiated when the in-plane compression is applied, see equation (6.3.1). This is also the reason that no clear buckling strain is observed in Figure 6.14.

$$\{M\} = [B]\{e\} + \cdots \qquad (6.3.1)$$

For the laminate with arbitrary initial imperfection, it starts deforming to a single half sine wave, and then the deformed shape changes to two half sine waves at progressive increase in end-shortening strain. The deformed shapes at four levels of applied end-shortening strain are shown in Figure 6.16. When the magnitude of imperfection increases, the laminate deforms to two half sine waves initially. Figure 6.17 shows the total deflection of the laminate at y = 25, 50 and 75.

To conclude, analysis of laminates with general initial imperfections has been evaluated. The post-buckling responses, influenced by the initial imperfection, may be different from those of flat laminate.

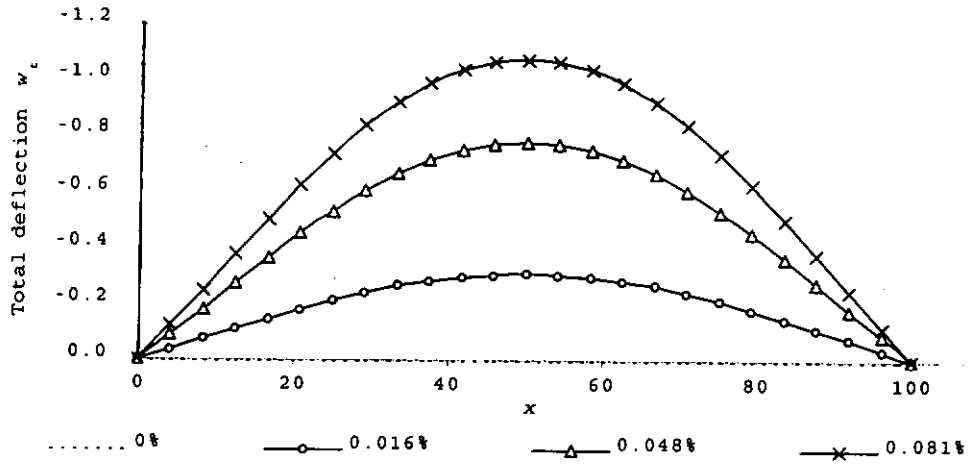

(a)

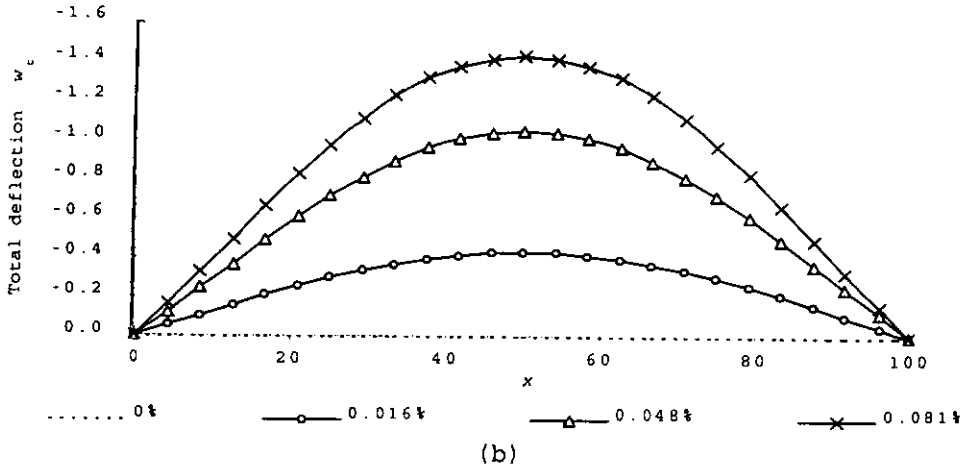

(b)

Figure 6.15 Flat unsymmetric cross-ply laminate: variations of w_t along the nodal lines, (a) y = 25 or 75 and (b) y = 50, at four levels of end-shortening strain

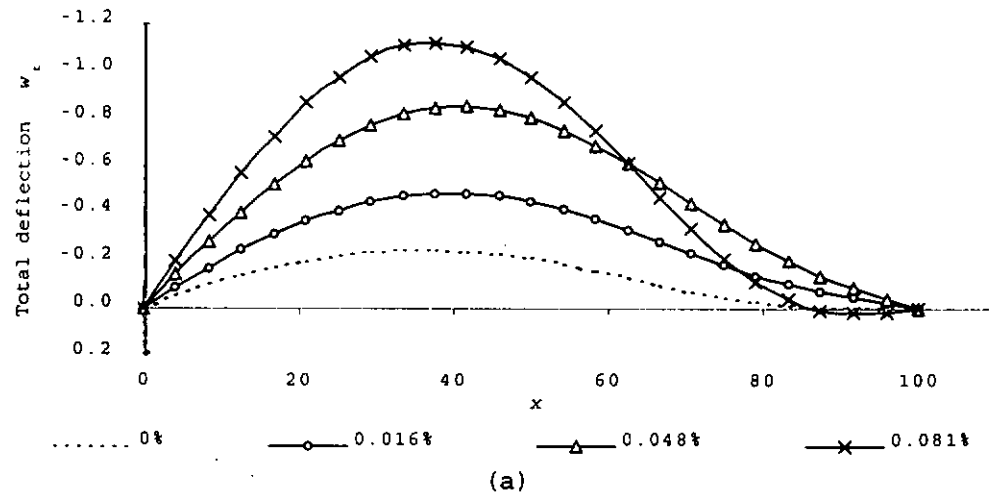

(a)

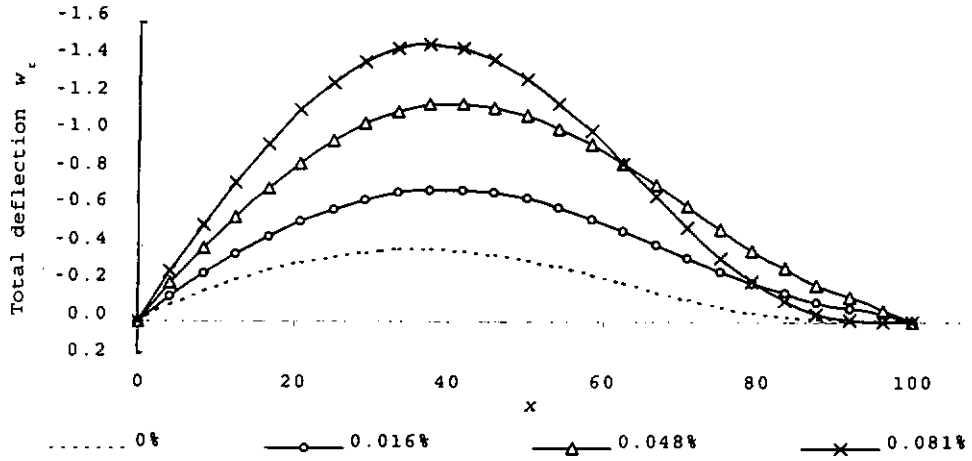

(b)

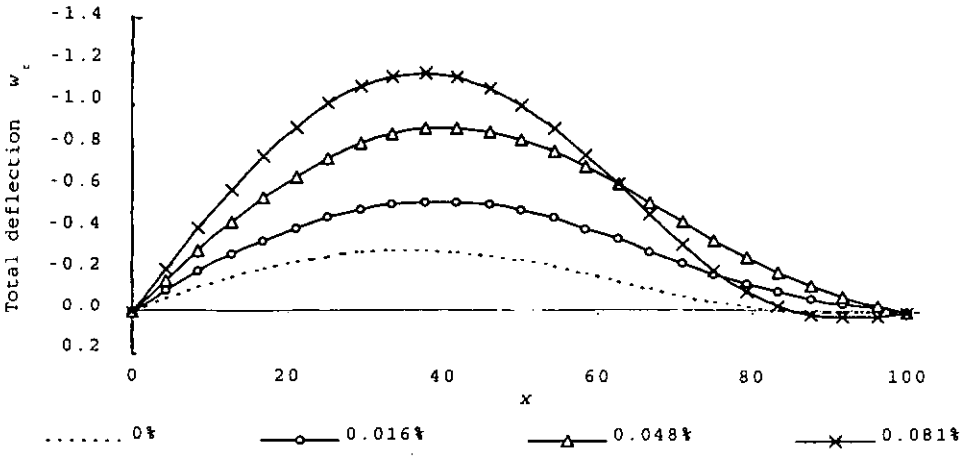

(c)

Figure 6.16 Unsymmetric cross-ply laminate with arbitrary initial imperfection: variations of w_t along the nodal lines, (a) y = 25, (b) y = 50 and (c) y = 75, at four levels of end-shortening strain

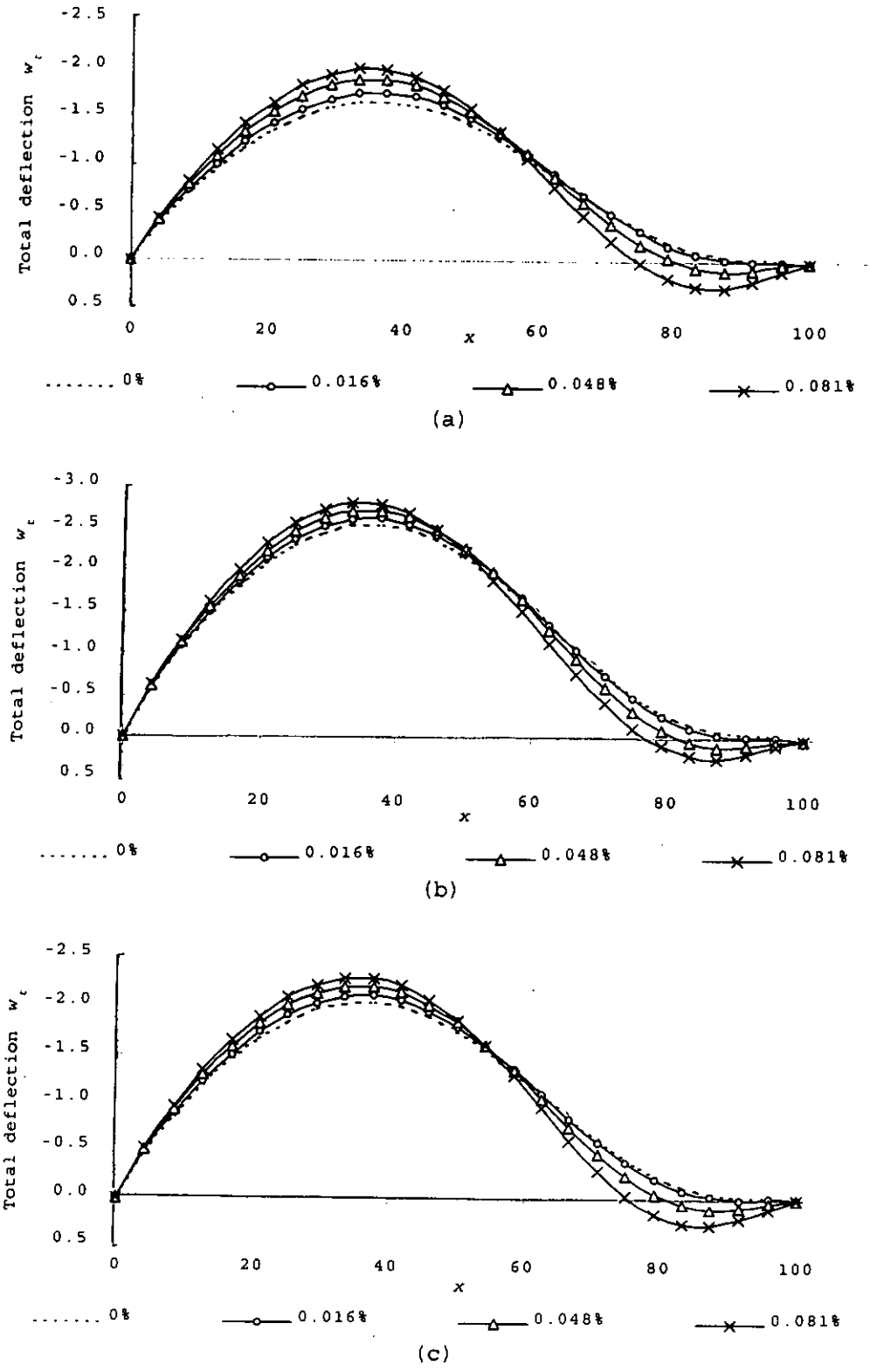

Figure 6.17 Unsymmetric cross-ply laminate with enlarged initial imperfection: variations of w_t along the nodal lines, (a) y = 25, (b) y = 50 and (c) y = 75, at four levels of end-shortening strain

6.4 RECTANGULAR 15-LAYER ANISOTROPIC LAMINATES

The laminate under consideration has a length of 400 mm, a width of 150 mm and a thickness of 2.25 mm. It is made of 15 layers of equal thickness and common material. The laminate layup is $[+60/-60/+30]_5$ and the material properties are E_L = 104 kN/mm^2, E_T = 8.9 kN/mm^2, G_{LT} = 5.5 kN/mm^2 and ν_{LT} = 0.32. It follows that all the A_{ij}, D_{ij} and the B_{11}, B_{16}, B_{22} and B_{26} stiffness coefficients are non-zero, i.e. material anisotropy and coupling are present. The problem is of Type B condition with the loaded ends (of width 150 mm) held against in-plane lateral expansion, whilst the longitudinal edges are free to expand. The laminate is simply supported for out-of-plane behavior around its boundary.

Analysis of a flat laminate with the above material properties has been presented by Dawe, Lam and Azizian (1992). Post-buckling response with three half sine waves was obtained at high level of strain. Dawe, Wang and Lam (1995) proposed an analysis of anisotropic laminate with the initial imperfection, equation (6.4.1), similar to the deformed shape of a flat laminate.

$$w_o = w_{oh} \sin \frac{3\pi x}{400} \sin \frac{\pi y}{150} \qquad (6.4.1)$$

In this application, the initial imperfection is in the form of a single half sine wave, as shown in equation (6.4.2), which is different from the deformed shape of flat laminate.

$$w_o = w_{oh} \sin \frac{\pi x}{400} \sin \frac{\pi y}{150} \qquad (6.4.2)$$

Both the present, with imperfection represented by polynomials, and previous, with exact imperfection, approaches can be applied for this application and very close results are expected. In this study, a fourth order polynomial function is used to simulate the longitudinal initial imperfection, as shown in equation (6.4.3).

$$\sin\frac{\pi x}{400} \cong 7.76\cdot 10^{-3}x + 3.01\cdot 10^{-6}x^2 - 1.12\cdot 10^{-7}x^3 + 1.40\cdot 10^{-10}x^4 \qquad (6.4.3)$$

In analyzing the behavior of this anisotropic laminate under end-shortening, a finite strip model with six quadratic finite strips over the whole plate is applied. The longitudinal series representation for u, v and w are sin 1-7, sin 1-7 and sin 1-5, respectively.

Values of w_{oh} being considered include ±2 and ±8. Comparisons are made with the results obtained for the analysis of a flat laminate. Figures 6.18 and 6.19 show the variations of average longitudinal loads and end-shortening strains for w_{oh} = ±2 and w_{oh} = ±8, respectively.

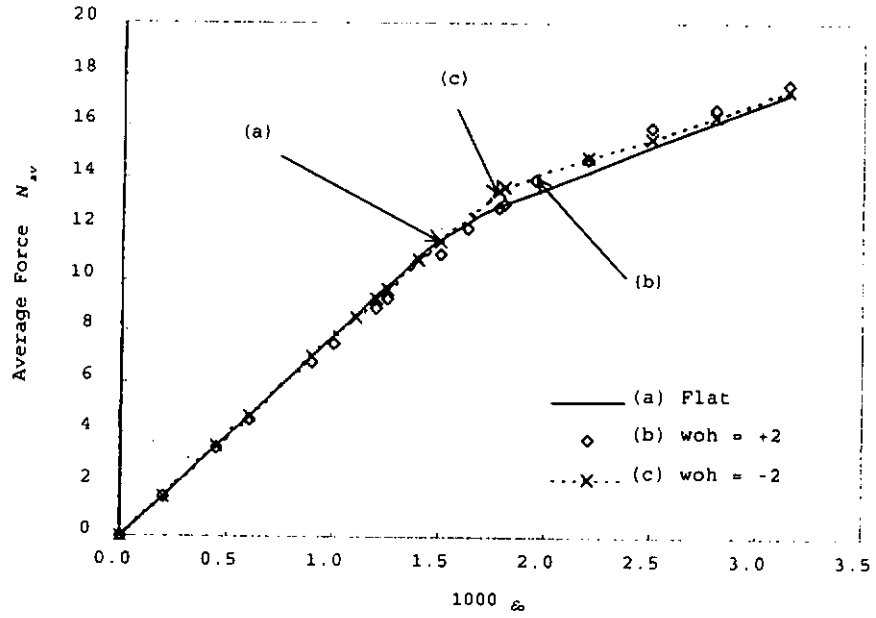

Figure 6.18 Rectangular 15-layer anisotropic laminates: variations of average force with end-shortening strain (w_{oh} = ±2); [In parentheses, (a) etc., denotes that the change to three half sine waves occurs]

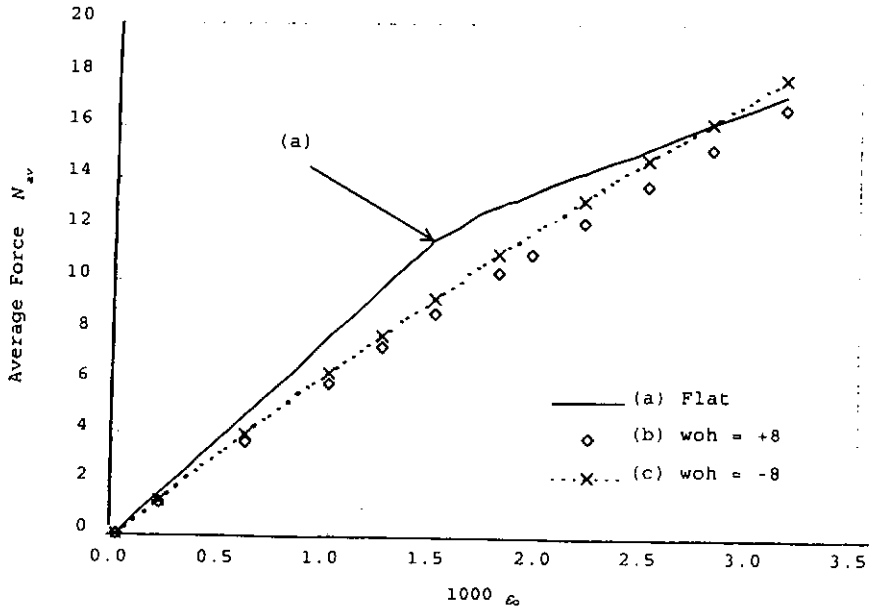

Figure 6.19 Rectangular 15-layer anisotropic laminates: variations of average force with end-shortening strain (w_{oh} = ±8); [In parentheses, (a) etc., denotes that the change to three half sine waves occurs]

For w_{oh} = ±2, the deformed shapes become three half sine waves at high level of end-shortening strain. Along the equilibrium paths in Figure 6.18, the changes in deformed shape of each imperfection are shown, of which coefficients of the sin 3 terms for out-of-plane displacement become dominant. For w_{oh} = ±8, the change in deformed shape does not occur within the range of progressive end-shortening strain up to ε_o = 0.315%, whilst the change can be observed around ε_o = 0.15% for flat laminate. The deformed shapes of laminates with w_{oh} = 0, ±2 and w_{oh} = 0, ±8 are shown in Figures 6.20 and 6.21, respectively.

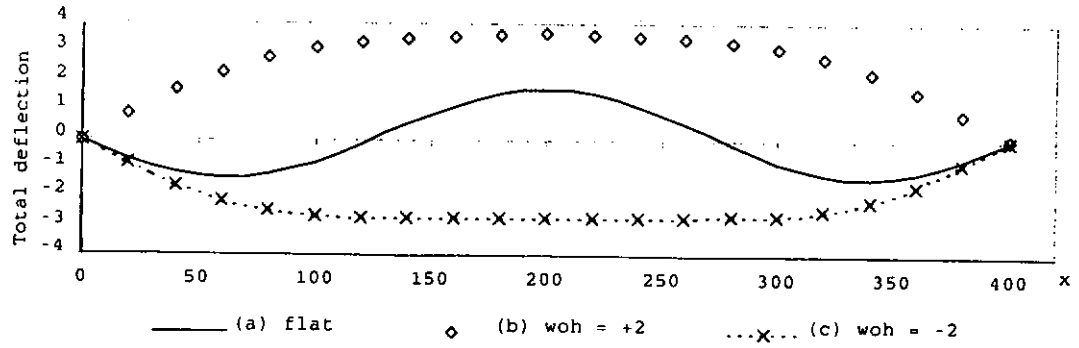

(a)

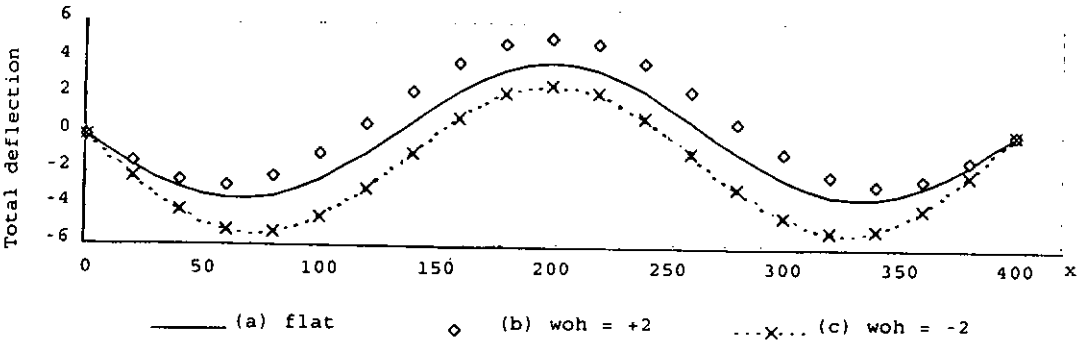

(b)

Figure 6.20 Rectangular 15-layer anisotropic laminates (w_{oh} = 0, ±2): variations of w_t at (a) ε_o = 0.180% and (b) ε_o = 0.315%

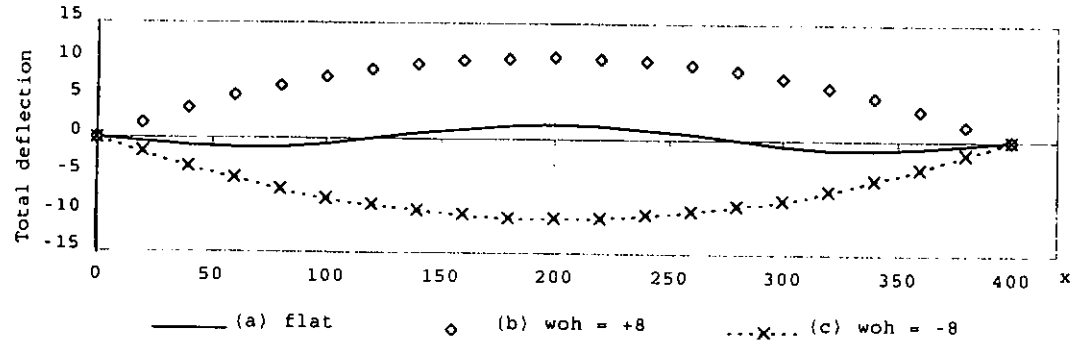

(a)

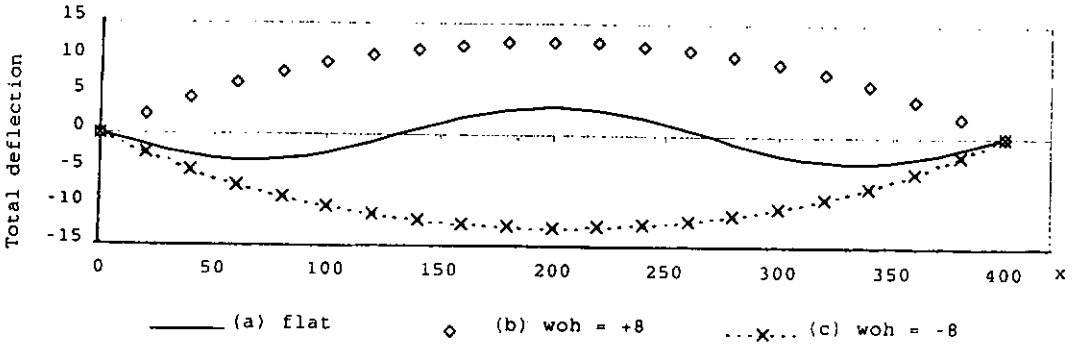

(b)

Figure 6.21 Rectangular 15-layer anisotropic laminates (w_{oh} = 0, ±8): variations of w_t at (a) ε_o = 0.180% and (b) ε_o = 0.315%

Figures 6.20 and 6.21 show that the deformed shapes are affected by the shapes and magnitudes of initial imperfections. The laminate deforms to three half sine waves with initial imperfection in form of three half sine waves, as demonstrated in previous study by Dawe, Wang and Lam (1995). However, it deforms to only a single half sine wave while the initial imperfection is in a single half sine wave with large magnitude.

CHAPTER 7

CONCLUSIONS AND RECOMMENDATIONS

7.1 CONCLUSIONS

Computational procedures for the post-buckling analysis of struts and plates with general initial imperfection when subjected to progressive end-shortening have been introduced. Suitable polynomial functions generated by the least-squares technique are used to simulate the initial imperfection, whilst the displacements are represented by Fourier series. Adaptability of such representations and efficiency of the approach have been verified through various applications. The results are compared with other available solutions. The technique is then applied to the analysis of isotropic and laminated plates with various forms of initial imperfections to assess the effects of imperfection.

7.1.1 Imperfect Struts

With the consideration of the transverse shear effect, formulation for the post-buckling analysis of struts has been developed. Both longitudinal and lateral displacements are represented by appropriate Fourier series. Shear locking effecting is alleviated due to the use of consistent order of representation for the variables w and β_x.

Initial imperfection in very general form is allowed. Approximations of the imperfection by suitable polynomial functions are obtained by using the least-squares technique. For symmetric imperfection expressed by trigonometric terms, the imperfection has

been approximated with respect to its magnitude or slope. When the form of imperfection is very general or is defined by discrete field measurements, the technique can also be applied to simulate the magnitude of imperfection. Applications on both cases have been performed. Close comparisons with other available solutions, of which the initial imperfection is expressed by trigonometric series, and from experimental results, by Lam (1998), are obtained.

In this study, both relatively thick and thin struts have been considered. The effect of transverse shear is observed to increase with the thickness of the strut. To conclude, the present approach is applicable for the analysis of struts with various forms of imperfection and thickness.

7.1.2 Imperfect Laminated Plates

In the context of classical plate theory, a finite strip approach has been developed for the post-buckling analysis of laminated plates. Consistent with both the in-plane and out-of-plane boundary conditions at the loaded ends, appropriate Fourier series and polynomial function are used to represent the displacements and initial imperfection along each longitudinal nodal line, respectively. The longitudinal functions are then interpolated by the crosswise polynomial functions within a finite strip.

Geometric non-linearity has been introduced in the strain-displacement equations in the manner of von Karman assumptions. Formulation involves general stress-strain relationships for laminates in the presence of coupling term for anisotropic material. For isotropic plate with symmetric initial imperfection, analytical solution by Yamaki (1959) and other finite strip solutions by Dawe, Wang and Lam (1995), of which the imperfection

is expressed in its exact form, are compared with the present solutions for verifying the present approach. Close comparisons have been recorded.

Other applications including isotropic plates, cross-ply laminates and laminates with general layup arrangement have been considered. In each application, different post-buckling responses are obtained while the initial imperfections are in different forms or magnitudes. The deformed shapes can be traced by the dominating terms in the displacement fields.

In conclusion, the present approach has provided a semi-analytical procedure to analyze the laminated plates with general initial imperfection when subjected to progressive end-shortening. The forms or magnitudes of imperfection influence the post-buckling response of laminated plates. In previous study, only trigonometric series was used to approximate the initial imperfection in the traditional finite strip method.

7.2 RECOMMENDATIONS

In this study, initial imperfections in very general form are simulated by appropriate polynomial functions. To fit the actual imperfection accurately, higher order polynomial functions may also be used. This leads to increasing computational effort, and longer computational time is required. The balance of accuracy and economy must be considered. In simple cases, solution based on imperfection represented by Fourier series would be acceptable. For other cases, the present approach provides accurate prediction when the initial imperfection is in very general form.

Further developments on the approach can also be considered. The first one is the analysis of laminated plates with general

initial imperfection, using shear deformation plate theory. To include the transverse shear strains (γ_{yz} and γ_{zx}), two fundamental components of displacement are introduced, which are the rotations (ψ_x and ψ_y) of the plate normals along the x and y directions. The second development is to extend the present approach to predict the buckling strength of plate structures, for example, cold-formed steel members.

REFERENCES

1. Allen, H. G. and Bulson, P. S. *Background to buckling*. McGraw-Hill, London ; New York (1980)
2. Atkinson, K., *An Introduction to Numerical Analysis*, Wiley, New York (1989)
3. Azhari, M. and Bradford, M. A. "The Use of Bubble Functions for the Post-local Buckling of Plate Assemblies by the Finite Strip Method". *Int. J. Numer. Methods Engng.*, Vol.38, pp.955-968 (1995)
4. Bradford, M. A. and Azhari, M. "The Use of Bubble Functions for Stability of Plates with Different End Conditions". *Engng. Struct.*, Vol.19(2), pp.151-161 (1997)
5. Cheung, Y. K. "The Finite Strip Method in the Analysis of Elastic Plates with Two Opposite Simply Supported Ends". *Proc. I.C.E.*, Vol.40, pp.1-7 (1968)
6. Cheung, Y. K. and Tham, L. G. *Finite Strip Method*. CRC Press, Boca Raton, Florida (1997)
7. Chia, C. Y. *Nonlinear Analysis of Plates*. McGraw-Hill, New York (1980)
8. Chia, C. Y. and Prabhakara, M. K. "Postbuckling Behavior of Unsymmetrically Layered Anisotropic Rectangular Plates". *J. Appl. Mech. Trans. ASME*, Vol.41, pp.155-162 (1974)
9. Chia, C. Y. and Prabhakara, M. K. "Nonlinear Analysis of Orthotropic Plates". *J. Mech. Engng. Sci.*, Vol.17, pp.133-138 (1975)
10. Cook, R. D., Malkus, D. S. and Plesha, M. E. *Concepts and Applications of Finite Element Analysis*. Wiley, New York (1989)
11. Crisfield, M. A. "A Fast Incremental/iterative Solution

Procedure that Handles Snap-through". *Comput. Struct.*, Vol.13, pp.55-62 (1981)

12. Dawe D. J., Lam, S. S. E. and Azizian, Z. G. "Non-linear Analysis of Rectangular Laminates under End Shortening, Using Classical Plate Theory". *Int. J. Numer. Methods Engng.*, Vol.35, pp.1087-1110 (1992)
13. Dawe D. J., Lam, S. S. E. and Azizian, Z. G. "Finite Strip Post-Local-Buckling Analysis of Composite Prismatic Plate Structures". *Comput. Struct.*, Vol.48(6), pp.1011-1023 (1993)
14. Dawe, D. J. and Wang, S. "Postbuckling Analysis of Thin Rectangular Laminated Plates by Spline FSM". *Thin-Walled Structures*, Vol.30, pp.159-179 (1998)
15. Dawe, D. J., Wang, S. and Lam, S. S. E. "Finite Strip Analysis of Imperfect Laminated Plates under End Shortening and Normal Pressure". *Int. J. Numer. Methods Engng.*, Vol.38, pp.4193-4205 (1995)
16. Elishakoff, I., Cai, G. Q. and Starnes, J. H. "Non-Linear Buckling of a Column with Initial Imperfection via Stochastic and Non-Stochastic Convex Models". *Int. J. Non-Linear Mech.*, Vol.29(1), pp.71-82 (1994)
17. Fraser, W. B. and Budiansky, B. "The Buckling of a Column with Random Initial Deflections". *J. Appl. Mech.*, Vol.36, pp.232-240 (1969)
18. Gallagher, R. H. "Finite Element Analysis of Geometrically Nonlinear Problems", In Yamada, Y. and Gallagher, R. H. eds., *Theory and Practice in Finite Element Structural Analysis: Proceedings of the 1973 Tokyo Seminar on Finite Element Analysis*, Tokyo, Japan, 5-10 November, 1973, pp.109-123 (1973)
19. Gierlinski, J. T. and Graves-Smith, T. R. "The Geometric Non-linear Analysis of Thin-walled Structures by Finite Strips".

Thin-Walled Structures, Vol.2, pp.27-50 (1984)

20. Gisvold, K. M., and Moe, J. "Buckling Analysis by Means of Non-Linear Programming". *Int. J. Numer. Methods Engng.*, Vol.2, pp.353-361 (1970)
21. Graves-Smith, T. R. and Sridharan, S. "A Finite Strip Method for the Post-Locally-Buckled Analysis of Plate Structures". *Int. J. Mech. Sci.*, Vol.20, pp.833-842 (1978)
22. Hancock, G. J. "Nonlinear Analysis of Thin Sections in Compression". *J. Struct. Eng. Div. ASCE*, Vol.107, pp.455-471 (1981)
23. Hinton, E. and Zienkiewicz, O. C. "A Note on a Simple Thick Finite Strip". *Int. J. Numer. Methods Engng.*, Vol.11, pp.905-907 (1977)
24. Hughes, T. J. R., Taylor, R. L. and Kanoknukulchai, W. "A Simple and Efficient Finite Element for Plate Bending". *Int. J. Numer. Methods Engng.*, Vol.11, pp.1529-1543 (1977)
25. Ikeda, K. and Murota, K. "Computation of Critical Initial Imperfection of Truss Structures". *J. Engng. Mech.*, Vol.116(10), pp.2101-2117 (1990)
26. Ikeda, K. and Murota, K. "Critical Initial Imperfection of Structures". *Int. J. Solids Struct.*, Vol.26(8), pp.865-886 (1990)
27. Kapania, R. K. and Raciti, S. "Recent Advances in Analysis of Laminated Beams and Plates, Part I: Shear Effects and Buckling". *AIAA J.*, Vol.27, pp.923-934 (1989)
28. Kapania, R. K. and Yang, T. Y. "Buckling, Postbuckling, and Nonlinear Vibrations of Imperfect Plates". *AIAA J.*, Vol.25, pp.1338-1346 (1987)
29. Lam, S. S. E. "Post-buckling Analysis of a Strut with General Initial Imperfection". *Int. J. Numer. Methods Engng.*, Vol.43,

pp.1017-1028 (1998)

30. Lam, S. S. E. and Dawe, D. J., "Nonlinear Analysis of Rectangular Laminated Plates under End Shortening Using the Finite Strip Method", In Leondes, C. T., ed., *Structural Dynamic Systems Computational Techniques and Optimisation Computer-Aided Design and Engineering*, Gordon and Breach Int. Series in Eng. Techniques and Appl. Sci., Vol.7, pp.143-175 (1998)

31. Lam, S. S. E., Dawe D. J. and Azizian, Z. G. "Non-linear Analysis of Rectangular Laminates under End Shortening, Using Shear Deformation Plate Theory". *Int. J. Numer. Methods Engng.*, Vol.36, pp.1045-1064 (1993)

32. Lam, S. S. E., Zou, G. P. and Lui, T. H., "Finite Strip Analysis of Laminated Plates under In-Plane Loads", In Choi, C. K. and Schnobrich, W. C., eds., *Proceedings of the First International Conference on Advances in Structural Engineering and Mechanics*, Vol.2, Seoul, Korea, 23-25 August, 1999, pp.1267-1272 (1999)

33. Lee, S.W. and Pian, T. H. H. "Improvement of Plate and Shell Finite Elements by Mixed Formulation". *AIAA J.*, Vol.16, pp.29-34 (1978)

34. Leissa, A. W. "A Review of Laminated Composite Plate Buckling". *Appl. Mech. Rev.*, Vol.40, pp.575-591 (1987)

35. Lui, T. H. and Lam, S. S. E. "Postbuckling Analysis of Plate with General Initial Imperfection by Finite Strip Method". In Chan, S. L. and Teng, J. G. eds., *Proceedings of the Second International Conference on Advances in Steel Structures*, Vol.2, Hong Kong, China, 15-17 December, 1999, pp.579-585 (1999)

36. Lui, T. H. and Lam, S. S. E., "Finite Strip Analysis of

Laminated Plates with General Initial Imperfection under End Shortening", *submitted to Engng. Struct.* (1999)

37. Mawenya, A. S. and Davies, J. D. "Finite Strip Analysis of Plate Bending Including Transverse Shear Effects". *Build. Sci.*, Vol.9, pp.175-180 (1974)

38. Minguet, P. J., Dugundji, J. and Lagace, P. "Postbuckling Behavior of Laminated Plates Using a Direct Energy-Minimization Technique". *AIAA J.*, Vol.27(12), pp.1785-1792 (1989)

39. Moy, S. S. J. and Lam, S. S. E. "A New Formulation for Plate and Shell Finite Elements". *Commun. Appl. Numer. Methods*, Vol.6, pp.457-470 (1990)

40. Novozhilov, V. V. *Foundations of the Nonlinear Theory of Elasticity*. Graylock Press, Rochester, N.Y. (1953)

41. Onate, E. and Suarez, B. "A Comparison of the Linear, Quadratic and Cubic Mindin Strip Elements for the Analysis of Thick and Thin Plates". *Comput. Struct.*, Vol.17(3), pp.427-439 (1983)

42. Prabhakara, M. K. and Chia, C. Y. "Post-Buckling Behaviour of Rectangular Orthotropic Plates". *J. Mech. Engng. Sci.*, Vol.15, pp.25-33 (1973)

43. Prathap, G. and Bhashyam, G. R. "Reduced Integration and the Shear-felexible Beam Element". *Int. J. Numer. Methods Engng.*, Vol.18, pp.195-210 (1982)

44. Riks, E. "An Incremental Approach to the Solution of Snapping and Buckling Problems". *Int. J. Solids Struct.*, Vol.15, pp.529-551 (1979)

45. Ryder, G. H. *Strength of Materials*. MacMillan, London (1969)

46. Saigal, S., Kapania, R. K. and Yang, T. Y. "Geometrically Nonlinear Finite Element Analysis of Imperfect Laminated Shells". *J. Composite Mater.*, Vol.20, pp.197-214 (1986)

47. Shen, H. S. and William, F. W. "Postbuckling Analysis of

Imperfect Composite Laminated Plates on Non-linear Elastic Foundations". *Int. J. Non-Linear Mech.*, Vol.30(5), pp.651-659 (1995)

48. Shiau, L. C. and Wu, T. Y. "A Finite Element Approach to Postbuckling Analysis of Laminated Plates", In Poursartip, A. and Street, K., eds., *Proceedings of the Tenth International Conference on Composite Materials*, Vol.5, Whistler, British Columbia, Canada, 14-18 August, 1995, pp.85-92 (1995)
49. Shin, D. K., Griffin, O. H. and Gurdal, Z. "Postbuckling Response of Laminated Plates under Unaxial Compression". *Int. J. Non-Linear Mech.*, Vol.28(1), pp.95-115 (1993)
50. Sridharan, S. and Graves-Smith, T. R. "Post-buckling Analysis with Finite Strips". *J. Eng. Mech. Div. ASCE*, Vol.107, pp.869-887 (1981)
51. Stein, M. "Effects of Transverse Shearing Flexibility on Postbuckling of Plates in Shear". *AIAA J.*, Vol.27(5), pp.652-655 (1989)
52. Stein, M. "Postbuckling of Orthotropic Composite Plates Loaded in Compression". *AIAA J.*, Vol.21(12), pp.1729-1735 (1983)
53. Stein, M. "Postbuckling of Long Orthotropic Plates in Combined Shear and Compression". *AIAA J.*, Vol.23(5), pp.788-794 (1985)
54. Timoshenko, S. and Gere, J. M. *Theory of Elastic Stability*. McGraw-Hill, New York (1961)
55. Whitney, J. M. "Shear Correction Factors for Orthotropic Laminates under Static Load". *J. Appl. Mech.*, Vol.40, pp.302-304 (1973)
56. Whitney, J. M. *Structural Analysis of Laminated Anisotropic Plates*. Technomic Pub. Co., Lancaster, Pa. (1987)
57. Whitney, J. M. and Pagano, N. J. "Shear Deformation in Heterogeneous Anisotropic Plates". *J. Appl. Mech.*, Vol.37,

pp.1031-1036 (1970)

58. Yamaki, N. "Postbuckling Behavior of Rectangular Plates with Small Initial Curvature Loaded in Edge Compression". *J. Appl. Mech. Trans. ASME*, Vol.26, pp.407-414 (1959)

59. Prathap, G and Babu, C. R. "A Field Consistent Three-noded Quadratic Curved Axisymmetric Shell Element". *Int. J. Numer. Methods Engng.*, Vol.23, pp.711-723 (1986)

60. Zienkiewicz, O. C. and Taylor, R. L. *The Finite Element Method.* Vol.1 & Vol.2, McGraw-Hill, London (1989)

61. Zienkiewicz, O. C., Taylor, R. L. and Too, J. M. "Reduced Integration Technique in General Analysis of Plates and Shells". *Int. J. Numer. Methods Engng.*, Vol.3, pp.275-290 (1971)

LIST OF PUBLICATIONS DURING STUDY

1. Lam, S. S. E., Zou, G. P. and Lui, T. H., "Finite Strip Analysis of Laminated Plates under In-Plane Loads", In Choi, C. K. and Schnobrich, W. C., eds., *Proceedings of the First International Conference on Advances in Structural Engineering and Mechanics*, Vol.2, Seoul, Korea, 23-25 August, 1999, pp.1267-1272 (1999)
2. Lui, T. H. and Lam, S. S. E. "Postbuckling Analysis of Plate with General Initial Imperfection by Finite Strip Method". In Chan, S. L. and Teng, J. G. eds., *Proceedings of the Second International Conference on Advances in Steel Structures*, Vol.2, Hong Kong, China, 15-17 December, 1999, pp.579-585 (1999)
3. Lui, T. H. and Lam, S. S. E., "Finite Strip Analysis of Laminated Plates with General Initial Imperfection under End Shortening", *submitted to Engng. Struct.* (1999)

APPENDIX A

LEAST-SQUARES APPROXIMATION FOR INITIAL IMPERFECTION

The least-squares technique is used for approximating the initial imperfection w_o frequently in this study. The polynomial function,

$$f(x) = \sum_{j=1}^{n} a_j x^j \qquad \text{(A.0.1)}$$

has been chosen to represent the exact $w_o = F(x)$. Because of the out-of-plane simply support boundary conditions, the coefficient a_0 usually vanishes.

A.1 INITIAL IMPERFECTION DEFINED BY A EXACT FUNCTION

The sum of square differences D between $F(x)$ and $f(x)$ is

$$D = \int [F(x) - f(x)]^2 dx \qquad \text{(A.1.1)}$$

A necessary condition for minimizing D is that

$$\frac{\partial D}{\partial a_j} = 0 \quad \text{for } j = 1, \ldots, n \qquad \text{(A.1.2)}$$

Since

$$D = \int (F(x))^2 dx - 2\sum_{j=1}^{n} a_j \int x^j F(x) dx + \int \left(\sum_{j=1}^{n} a_j \right)^2 dx \qquad \text{(A.1.3)}$$

$$\frac{\partial D}{\partial a_j} = -2\int x^j F(x)dx + 2\sum_{k=1}^{n} a_k \int x^{j+k}dx \qquad \text{(A.1.4)}$$

$$\sum_{k=1}^{n} a_k \int x^{j+k}dx = \int x^j F(x)dx \qquad \text{(A.1.5)}$$

Therefore, the coefficients a_j can be obtained by solving the linear system in equation (A.1.6).

$$[\boldsymbol{L}_C]\{\boldsymbol{a}\} = \{\boldsymbol{f}_C\} \qquad \text{(A.1.6)}$$

where $[\boldsymbol{L}_C] = [L_{ij}]$ is a $n \times n$ square matrix, $\{\boldsymbol{a}\} = \{a_j\}$ and $\{\boldsymbol{f}_C\} = \{f_j\}$ are $n \times 1$ column vectors, for $i, j = 1, \ldots, n\text{-}1, n$.

$$L_{ij} = \int x^{i+j}dx \qquad \text{(A.1.7)}$$

$$f_j = \int x^j F(x)dx \qquad \text{(A.1.8)}$$

A.2 INITIAL IMPERFECTION DEFINED BY DISCRETE MEASUREMENTS

In this case, $w_o(x)$ is not defined as a known function. Only discrete values $w_o(x_k)$ are measured. The sum of square differences D between $F(x)$ and $f(x)$ becomes

$$D = \sum_k [w_o(x_k) - f(x_k)]^2 \qquad \text{(A.2.1)}$$

Also with the condition in equation (A.1.2) and following the similar procedures, a linear system can be formed.

$$D = \sum_k (F(x_k))^2 - 2\sum_{j=1}^{n} a_j \left(\sum_k F(x_k) x_k^j \right) + \sum_{j=1}^{n}\sum_{m=1}^{n} a_j a_m \left(\sum_k x_k^{j+m} \right) \qquad \text{(A.2.2)}$$

$$\frac{\partial D}{\partial a_j} = -2\sum_k F(x_k)x_k^j + 2\sum_{j=1}^{n} a_j \sum_k x_k^{j+m} = 0 \qquad \text{(A.2.3)}$$

$$\sum_{j=1}^{n} a_j \sum_k x_k^{j+m} = \sum_k F(x_k)x_k^j \qquad \text{(A.2.4)}$$

Coefficients a_j can be obtained by solving (A.2.5).

$$[L_D]\{a\} = \{f_D\} \qquad \text{(A.2.5)}$$

This linear system is similar as the one in Chapter A.1. However, the entries in the square matrix $[L_D] = [L_{ij}]$ and the right hand side vector $\{f_D\} = \{f_j\}$ are different.

$$L_{ij} = \sum_k x_k^{i+j} \qquad \text{(A.2.6)}$$

$$f_j = \sum_k F(x_k)x_k^j \qquad \text{(A.2.7)}$$

A.3 APPROXIMATION OF THE SLOPE OF INITIAL IMPERFECTION

In order to simulate the slope of w_o in Chapter 2.2, it is easy to replace the equation (A.0.1) by

$$f(x) = \sum_{j=1}^{n} j a_j x^{j-1} \qquad \text{(A.3.1)}$$

and

$$F(x) = \frac{dw_o}{dx} \qquad \text{(A.3.2)}$$

and then follows the procedures in the Chapters A.1 or A.2. The coefficients a_j ($j = 1, \ldots, n$) can be solved and a_0 is zero for the simply support condition.